Development of an unbiased methodology to quantify pathological changes in the respiratory tract

Thesis submitted in fulfilment of the requirements of the University of Glasgow for the degree of Master in Veterinary Medicine

By

Veronica Ann Patton
DVM, MRCVS
School of Veterinary Medicine,
College of Medical, Veterinary and Life Sciences

September 2020

Abstract

Histopathological analysis applies to a variety of situations (diagnostics, sudden deaths, controversial cases, infectious diseases, intoxications amongst others) and, if achieving a diagnosis is considered the ultimate aim in most of the cases, when it comes to more exquisitely experimental fields, the simple assessment of presence/absence of alterations is considered not sufficient.
For this reason, the need of a rigorous evaluation of the samples had initially pushed to the development of scoring systems (aka 'grading') which however remain only partially beneficial and produce data of exclusively semi-quantitative nature.
The advent of several image analysis software programs has overcome this limitation and opened the way to convert images into proper measurements which in turn are suitable to further statistical analysis.

In my thesis, I wanted to develop a consistent method to quantify pathological changes.
For this purpose, I decided to test ImageJ on a thoroughly characterised and largely used *ex vivo* organ culture (EVOC) system represented by horse tracheal explants infected with equine influenza virus (EIV). Whether the traditional histopathological scoring should be regarded as a valid complementary tool, ImageJ allowed to consistently measure different stainings (pixel quantification) and nuclear parameters (particles count; nuclear area) and to avoid the need of a second operator to validate the analysis.

In conclusion, quantification of pathological changes by means of image analysis software not only is feasible, but also provides with unbiased data and highlights even the more subtle changes that would otherwise be unapparent by eye via traditional scoring approach.

Index

List of tables

List of figures

Acknowledgments

I would like to express my deepest gratitude to Dr Pablo Murcia for giving me the opportunity to join his group during my Research Master and to be exposed to such a stimulating and innovative environment as the Centre for Virus Research.

Special thanks go to Daniel Goldfarb who specifically designed the macros used in my thesis and patiently trained me on how to the use ImageJ.

Special thanks go to Julien Amat for always being supportive and for the invaluable help provided with statistical analysis.

Thanks to the histopathology lab (Lynn Stevenson, Lynn Oxford, Frazer Bell) for their amazing technical work.

Thanks to the pathologists (my supervisor Dr Angie Rupp, Dr Pamela Johnston, Dr Caroline Millins, Dr Alex Gray, Dr Francesco Marchesi) for always being supportive.

Thanks to the anatomic pathology residents, the old and the new ones (Virginia, Livia, Gail, Marta, and Kate), for sharing the joy and the pain of this incredible adventure called residency.

Thanks to the 'Ilarias' (Ilaria Piras, and Ilaria Epifano) for their friendship.

And finally, special thanks to my family, Francesco and Matilde, for always being by my side.

Author's Declaration

I, Veronica Ann Patton, declare that, except where explicit reference is made to the contribution of others, this dissertation is the result of my own work and has not been submitted for any other degree at the University of Glasgow or any other institution.

Veronica Ann Patton

List of Abbreviations

CC3	Cleaved Caspase-3
DAB	3, 3-diaminobenzidine
dpi	day post infection
EIV	Equine Influenza Virus
EIVs	Equine Influenza Viruses
EVOC	*ex vivo* Organ Culture (System)
HA	Hemagglutinin
H&E	Haematoxylin and Eosin
IHC	Immunohistochemistry
NA	Neuraminidase
NP	Nucleoprotein
pfu	plaque forming unit
PB2	Polymerase Basic Protein 2
RdRp	RNA-dependent RNA polymerase
RIPK3	Receptor-Interacting Serine/Threonine-Protein Kinase 3
vRNPs	viral Ribonucleoprotein Complexes
VDS	Veterinary Diagnostic Service

1 General introduction

1.1 Pathological changes and diseases

'Pathology' - from Ancient Greek πάθος (páthos, "suffering") and -λογία (-logía, "study") literally means 'the study of suffering'. In more pragmatic words, pathology as a discipline consists of the study of diseases particularly with regards to their intrinsic features and manifestations and possible underlying causal agents (Mitchell, 2014).

Depending on the nature of the aetiology, the organ and tissue changes caused by diseases are assessable either macroscopically by direct inspection and/or microscopically by histological evaluation.

Pathological/histopathological analysis can be applied to a variety of situations including naturally occurring diseases, forensic cases, anaesthetic/unexpected deaths, experimental disease/infection, toxicopathology, and telepathology (Grant Maxie & Miller, 2016). The ultimate goal of the pathologist is to provide with a diagnosis which in turn may provide with a reliable explanation for the disease, discomfort, or even death of the individual submitted to post-mortem examination and to prevent and control further spread of infectious conditions, but also to identify newly emerging diseases, or, particularly in case of affection animals, to clarify the underlying conditions leading to death (Grant Maxie & Miller, 2016).

Whatever the application would be, a crucial concept appears to be the so-called 'pattern of recognition', attributed to Ackerman (Ackerman, 1978) and mostly applied to the dermatopathology context, but equally applicable to histopathology of systems and organs other than skin and also in the experimental settings. Gross, subgross, and microscopic patterns of recognition can be described as the steps ultimately required to sort out the observed pathological changes into categories with the purpose to reach few final differential diagnoses, if not the specific underling aetiology.

1.2 Quantifying disease severity

1.2.1 Is it possible to quantify pathological changes in an unbiased way?

In most applications of histopathology, the assessment of lesions and associated patterns of recognition is more than enough to make a diagnosis, but when it comes to experimental disease/infection or even in the diagnostic settings with the ultimate goal of making a reliable prognostication and/or defining an appropriate clinical management/therapeutic schedule – and here a classic example is represented by staging of liver biopsies in horses (Durham, et al., 2003) - the pathologist is called not only to assess the presence/absence of morphologic alterations in the selected tissues, but also to highlight differences amongst experimental groups and, in the case of diagnostics, to judge the severity of the processes, in other words to define the extension (magnitude) of the lesions. For this reason, the need of a rigorous evaluation of the samples had

pushed to the development of scoring systems (aka ‘grading’) where semiquantitative data can be obtained from the examined tissues for subsequent group comparison (Gibson-Corley, Olivier, & Meyerholz, 2013).

According to Crissman and colleagues (Crissman, Goodman, Hildebrandt, & al, 2004), there are three requirements to make a reliable scoring system:

- it has to be identifiable;
- it has to be reproducible, and
- it must produce meaningful results.

An exhaustive comprehension of the experimental set with related objectives and methods is thought to be the essential requirement before the tissue analysis and development of a meaningful scoring system occur (Brayton, et al., 2001; Brayton, et al., 2012; Seller, 2012; Zeiss, et al., 2012).

Once the scoring method (in terms of selection of the tissues to be examined, lesions to be identified, and definition of the scores) is settled, in order to obtain results as unbiased as possible, a blind analysis of the samples obtained from the different groups and, when possible, analyses conducted by at least 2 independent operators are required with the purpose to obtain consistent and reproducible results (Shott, 2011).

One of the main limitations in the use of a grading system, besides to a proper validation of the system itself, is that this type of analysis always produces semi-quantitative data (e.g. nominal, ordinal, interval, and ratio data) as represented in Table 1.1 (adapted from Gibson-Corley).

Nowadays, the advent of several image analysis software able to convert images into measurements has opened the way to automatic identification of the pathological changes in organs/tissues.

Whether the role of the pathologist is irreplaceable for setting up the software, the computer-based image analysis not only has overcome the intrinsic biases of semi-quantitative scoring but has also supplied with reliable measurements which in turn are suitable to proper further statistical analysis. Once the data are obtained, the role of the pathologist however remains essential for the interpretation and validation of the results (Grant Maxie & Miller, 2016).

As a very general example, the presence of necrosis in a tissue can be detected either grossly by eye or microscopically and, based on the distribution (e.g. random, perivascular, multifocal, focally extensive) of the lesions, the pathologist can speculate on the most plausible origin of the lesions (e.g. infectious, toxic, or ischaemic injury).

However, it is through the use of image analysis software that the magnitude of the event either as numbers of necrotic foci and/or percentage of affected tissue can be determined in a proper quantitative way.

Table 1.1 Types of semiquantitative measurements.
Adapted from Gibson-Corley et al. (2013)

Types	Definition	Examples
Nominal	Samples assigned to a category in the absence of any reference to severity	Binary – presence or absence of viral antigen
Ordinal	Samples assigned to a category with an ordered progression in severity	0 – no necrosis 1 – mild necrosis 2 – moderate necrosis 3 – severe necrosis

1.2.2 A quantitative methodology to measure pathological changes

The overall aim of this thesis was to develop a consistent method to quantify pathological changes which ultimately would be applicable to naturally occurring diseases, ranging from infections through degenerative diseases to neoplastic processes.

For this purpose, I used ImageJ, a freely downloadable image analysis program and tested its applicability on a thoroughly characterised and largely used *ex vivo* organ culture (EVOC) system represented by horse tracheal explants infected with equine influenza virus (EIV).

1.2.3 ImageJ

ImageJ is an image analysis software developed at the National Institutes of Health and the Laboratory for Optical and Computational Instrumentation (LOCI, University of Wisconsin) which has been firstly released in 1997 (Schneider et al., 2012; Collins, 2007).

The program is compatible with the vast majority of the current operating systems (including Microsoft Windows, Mac Os, Linux). Many image file formats (including TIFF, PNG, GIF, JPEG, BMP, DICOM, and FITS), as well as raw formats, in addition to 8-bit colour and grayscale, 16-bit integer, and 32-bit floating point images can be processed by the program (Wikimedia Foundation Inc., 2020).

Measurements are performed in pixel numbers and if required subsequently converted in length, area, or volume by means of simple equations.

Additionally, throughout the creation of density histogram, the intensity of specific staining such as those produced by immunohistochemistry and immunofluorescence can be evaluated in a quantitative way.

Given the overt adaptability of ImageJ in addition and its free availability, I decided to use this software with the ultimate aim of developing a reliable unbiased quantitative method to quantify pathological changes and lesions.

1.3 Experimental system

1.3.1 Tissues

I used archived formalin-fixed paraffin embedded equine tracheal explants prepared by Alice Coburn for her post graduate doctoral degree (Coburn A. M., 2017). Explants had been prepared as per description of Nunes, et al. (2010) and Gonzalez, et al. (2014). Briefly, tracheas were collected from research ponies euthanised on welfare grounds (congenital cardiac abnormalities). Following aseptic collection immediately upon euthanasia, the tissues were transported to the laboratory and opened to allow the removal of the mucosa from the underlying cartilage. The airway epithelium, including the mucosa and submucosa but excluding the cartilage, was cut into small explants (approximately 0.5 by 0.5 cm) and placed in an air-liquid interface culture system in six-well plates with the purpose of mimicking the respiratory tract environment. Steps are summarised in Figure 1.1.

Explants were then infected with 200 plaque forming unit (pfu) of various EIVs, and collected at different time points post infection (1, 2, 3, 4, 5 day post infection). Subsequently, infected and control explants were placed in formalin and processed for further histopathological assessment.

For my research project, I first focused the investigation on a restricted number of samples and for this reason, explants infected with only one EIV were selected and compared with mock infected explants.

Figure 1.1 Equine tracheal explant preparation.

The trachea is removed immediately upon euthanasia (A). Small (approximately 0.5 x 0.5 cm) fragments of mucosa are removed from the underlying cartilage and placed in an air-liquid interface six-well plate (B). The fragments are collected at different time points post infection and following adequate fixation (<24 h in buffered 4% formalin) paraffin blocks and slides are obtained (C). Finally, the slides are stained for Haematoxylin and Eosin and immunohistochemistry (D).

Figure adapted from Julien Amat.

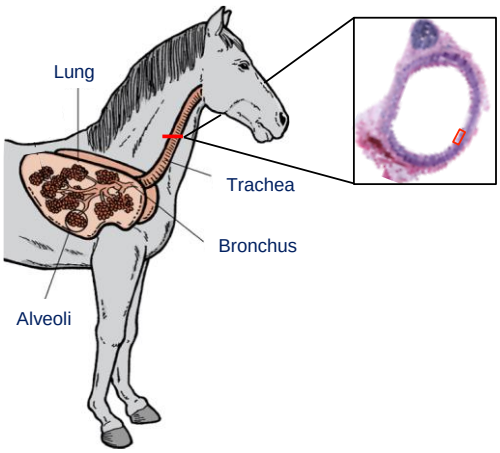

A

B

C

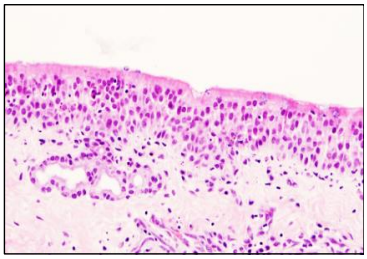

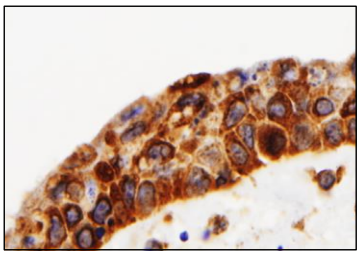

D

1.3.2 Equine Influenza

Equine Influenza is caused by equine influenza viruses (EIV) (Brown, 2000; Webster, et al., 1992). EIV has originated from avian influenza viruses (Caswell & William, 2016) and aquatic birds represent the natural reservoir for these viruses.

The viruses can be identified by the surface glycoproteins hemagglutinin (HA) and neuraminidase (NA). There are currently 18 HA and 11 NA and their presence on the virus surface is used for subtype classification. All the currently circulating EIVs are H3N8.

The disease is characterised by high morbidity – particularly in naïve populations with nearly 100% of the animals infected – and relatively low mortality. Fatal cases are largely caused by supervening secondary bacterial pneumonia (Caswell & William, 2016).

The upper respiratory airway and trachea are the sites where the viral replication occurs. Impairment of cilia resulting in reduced mucociliary clearance facilitates viral spread and invasion and to some extent also promote opportunistic bacterial infection.

Macroscopic and microscopic lesions of primary EIV infection are exceedingly rarely seen in naturally occurring cases because the disease usually completely resolves in a relatively short timeframe.

In experimentally infected horses, histopathological changes included rhinitis and tracheitis, with multifocal necrosis, loss of the superficial ciliated epithelium, and loss of goblet cells at early time points after the infection. Regenerative changes in terms of hyperplasia and squamous metaplasia of the respiratory epithelium were appreciable at the latest timepoints. However, late timepoints were also associated with suppurative bronchopneumonia caused by opportunistic bacterial infection (Muranaka, et al., 2012).

2 Objectives

2.1 Main purpose

The main purpose of this thesis was to develop an unbiased methodology to quantify pathology in respiratory tissues.

2.2 Objectives

- Description of pathological changes in tracheal explants due to EIV infection
- Description of immunohistochemical changes in tracheal explants due to EIV infection
- Semiquantitative analysis of immunohistochemical changes
- Semiquantitative analysis of histopathology
- Development of a quantitative image analysis pipeline using ImageJ
- Quantification of immunohistochemical changes.
- Quantification of histopathological changes.

3 Materials and Methods

3.1 Horse tracheal explants

3.1.1 Tissue preparation

Horse tracheal explants were prepared by Alice Coburn (Coburn A. M., 2017) for her post graduate doctoral degree as per description in Nunes et al. (2010) and Gonzalez et al. (2014).

Briefly, tracheas were collected from horses euthanised on welfare ground due to congenital cardiac abnormalities and transported to the lab in transport medium. Following a longitudinal incision, the mucosa was removed from the underlying cartilage and subsequently cut into approximately 0.5 by 0.5 cm squares. Two replicates were generated for every single timepoint in order to confirm repeatability and to increase consistency.

The explants were placed in a six well plates with an air-liquid interphase with the purpose of recreating an environment resembling the normal respiratory tract.

Explants were then infected with 200 plaque forming unit (pfu) of different strains EIV, collected at different time points post infection (1, 2, 3, 4, 5 dpi), and placed in formalin for histological analysis with the purpose of evaluating pathological changes associated with EIV infection. For this research project, I used the explants derived from a single horse and infected with A/equine/Ohio/2003 and mock-infected controls. Two replicates of mock and EIV infected explants (with exception of replicates 1 of mock explants at day 1 and 4 respectively) were evaluated at 5 different timepoints (day 1, 2, 3, 4, 5) for a total of 18 explants.

3.1.2 Haematoxylin & Eosin and Immunohistochemistry

Explants were fixed in 10% buffered formalin for up to 48 hours and then sent to the Veterinary Diagnostic Service (VDS) for embedding in paraffin blocks and sectioning. When the processing of the samples was not possible within 48 hours of fixation, in order to preserve tissue antigenicity without affecting tissue morphology, samples were transferred in 70% ethanol solution.

Five µm sections were cut from selected samples (mock and EIV infected explants) and stained with haematoxylin and eosin (H&E) or immunostained with different antibodies (see below). H&E staining was performed by VDS.

For immunohistochemistry, sections were rehydrated and placed in water. For cleaved caspase-3 (CC3) and KI67, antigen retrieval was performed by pressure cooker heating in citrate buffer (pH6). For nucleoprotein (NP), permeabilization was carried out following incubation with 0.01% Triton X in PBS for 10 minutes at room temperature. All sections were washed 3 times in 0.05% Tween 20 PBS (PBS/T) and incubated in a peroxidase blocking solution (H_2O_2 Sigma diluted 1/10 in PBS) for 10 minutes at room temperature. After 3 washes in PBS/T, sections were blocked with 10% normal goat serum in PBS/T for up to 30 minutes at room temperature. The blocking solution was also used to dilute the antibodies which in turn were incubated overnight at 4°C. After 3 washes in PBS/T, Dako EnVision system (K4001; K4003) was incubated as per instructions of the manufacturer

and the antigens detected with Dako DAB (3, 3 -diaminobenzidine) plus Substrate Chromogen System (K3467).

Antibodies specifications and dilutions are reported in table 3.1.

Finally, slides were counterstained by the histology service with Mayer's haematoxylin and mounted.

Table 3.1 Antibodies used for IHC.

Detected antigen, type, source, and working dilutions for antibodies used for this thesis are reported. NP rabbit polyclonal was custom made by GenScript®.

Primary Antibody	Monoclonal/Polyclonal	Source	Catalogue No.	Working Dilution
NP	Rabbit Polyclonal	GenScript (custom made)	Na	1/400
CC3 (Asp175)	Rabbit Polyclonal	Cell Signalling	#9661	1/400
Ki67	Mouse Monoclonal	DAKO	M7240	1/150

3.2 Semiquantitative scoring

For the semiquantitative scoring, a blind analysis was conducted twice to increase consistency and repeatability and was performed for both H&E and immunohistochemically stained slides.

3.2.1 Histological analysis

Criteria for histological evaluation were selected based on pathological changes seen in horses experimentally infected with EIV (Muranaka, et al., Time-related Pathological Changes in Horses Experimentally Inoculated with Equine Influenza a Virus, 2012) and included loss of ciliated and Goblet cells, attenuation of the respiratory epithelium, presence of individual or clustered apoptotic cells, and presence of mitotic figures which in turn were evaluated adopting a binary approach (presence or absence of each feature). Particularly with regards to apoptotic cells, the criteria for inclusion were cellular individualisation/separation from the adjacent viable cells, with shrunken cytoplasm, not unfrequently surrounded by an optically empty halo, in conjunction with cytoplasmic hypereosinophilia and shrunken (pyknotic) to on occasion fragmented (karyorrhectic), deeply basophilic nucleus.

3.3 Immunohistochemistry

3.3.1 NP and CC3 scoring

For NP, a binary approach (presence/absence of the staining) similar to that described for H&E sections was elected. For CC3, an ordinal approach was attempted based on subjectively estimated % of positivity over the explant epithelium length, taking into account the staining pattern and explant/tissue heterogeneity (sporadic apoptotic cells vs clusters of apoptotic bodies/apoptotic cells) in relation to timepoints (early vs late endpoints) (Janke, J.M., & P., 2019).
A semiquantitative score ranging from 0 to 2 was subsequently assigned to each explant.
Semiquantitative scoring of CC3 is reported in table 3.2.

Table 3.2 Semiquantitative scoring of CC3.

A score from 0 to 2 is assigned based on subjectively estimated percentage (%) of positivity (of sporadic apoptotic cells and clusters of apoptotic bodies/apoptotic cells) over the length of the tracheal epithelium.

CC3 positive cells	Estimated % of positivity	Assigned score
No	0	0
Sporadic apoptotic cells	<5	0.5
Clusters of apoptotic bodies/apoptotic cells	>5 but <10	1
Clusters of apoptotic bodies/apoptotic cells	>10	2

3.3.2 KI67 scoring

For KI67, a 'manual' count on randomly selected fields was performed at high power magnification (400x). The number of positive nuclei was counted on a total of 100 epithelial nuclei. Therefore, a percentage of nuclear positivity was calculated.

3.4 Quantitative scoring

All the histological images submitted for image analysis were collected using cellD* Software (Olympus). For each antibody used and for each timepoint, 3 photomicrographs at 400x magnification were taken from the central portion of the sections from mock and EIV infected explants in order to avoid crash artefacts generated by sampling and mostly evident at the edges of the slices. Specific macros for the quantification of NP, CC3, and Ki67 within the respiratory epithelium were developed by Daniel Goldfarb using ImageJ software (Version:2.0.0-rc-65/1.51w). The respiratory epithelium was manually selected. This procedure allowed to exclusively restrict the analysis to the epithelial compartment. Following colour deconvolution of the cropped epithelium, the picture generated in the DAB channel was converted in a binary picture (black and white), and the amount of positive signal was measured in terms of number of stained pixels. The number of pixels obtained for each marker was then normalised by the length of the explants (once again manually determined by me using the measuring function of ImageJ). This step was thought to be crucial, allowing to overcome the bias generated by the different orientation of the sections on the slides (vertical vs horizontal vs diagonal orientation), overall increasing the consistency of the quantification method. In addition, within all the micrographs processed for IHC analysis, in the H&E channel, the total number of epithelial nuclei was calculated together with the area covered by nuclei (nuclear area).
All the measurements were exported to an Excel spreadsheet to generate graphs and analyse the dynamics of the marker expression/nuclear count/nuclear area following EIV infection.
The quantification steps are shown in Figure 3.1.

Figure 3.1 IHC quantification using ImageJ.

The most salient steps of IHC signal quantification in the respiratory epithelium are summarised as follows. Three pictures were taken from each stained slide at high power field (40x) (A). The respiratory epithelium was manually selected and cropped (B). Following colour deconvolution, the positive signal was extracted in the DAB channel (C). The obtained picture is then converted to a binary (BW) picture, and the number of pixels quantified (D). For all the pictures analysed, in the H&E channel (E), the total number of nuclei (and the area covered by nuclei) was extracted and quantified (F). All the measurements were exported into an Excel spreadsheet (G). The data were then used to generate graphs to analyse the dynamics of marker expression/nuclear count/nuclear area following EIV infection (H).

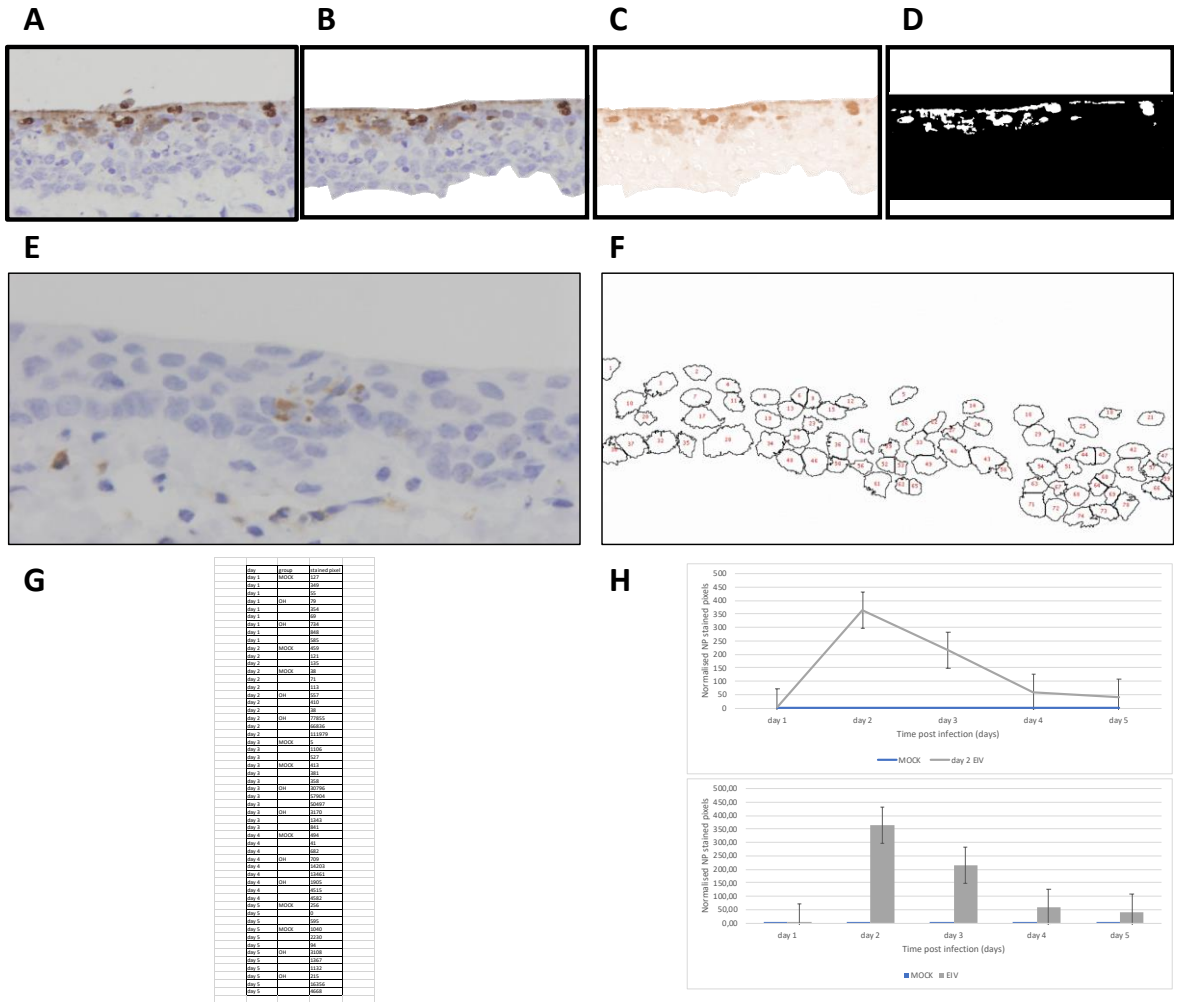

3.5 Statistical analysis

Results were reported as means plus standard errors of the means of three independent measurements for each sample. The non-parametric test Wilcoxon Mann Whitney was elected for the statistical analysis of the obtained data and differences between mock and EIV infected explants were considered significant when P was equal to 0.05 and highly significant when P was equal to 0.001.

4 Results

4.1 Histological changes due to EIV infection

Equine tracheal explants have been largely demonstrated to represent a relevant *ex vivo* organ culture (EVOC) system to study viral infections in the respect of the 3 Rs (Replacement Reduction and Refinement) as they retain all the histological features of a normal respiratory mucosa, including a pseudostratified ciliated columnar epithelium with scattered Goblet cells (Figure 4.1A). The samples used in this study were archived tracheal explants from a previous research project (Coburn A. M., 2017).

In first instance, I wanted to assess the presence of histopathological changes ascribable to EIV infection in H&E stained slides selected on the basis of pathological changes seen in horses experimentally infected with EIV (Muranaka, et al., Time-related Pathological Changes in Horses Experimentally Inoculated with Equine Influenza A Virus, 2012).

Lesions induced by the virus were qualitatively/semiquantitatively assessed in all the samples and included cellular loss, epithelial degeneration, and epithelial regeneration.

Cellular loss was evident in terms of overall loss of outer ciliated epithelial cells and reduction in the numbers of Goblet cells (mucinous cells) leading to thinning of the normal respiratory (pseudostratified ciliated columnar) epithelium (Figure 4.1B). In all the examined sections, however, there was no obvious evidence of ulceration). Epithelial degeneration was highlighted by multifocal flattening and attenuation of the suprabasal layer of respiratory epithelium and concurrent increase in the number of apoptotic epithelial cells, either as individualised apoptotic cells or grouped in small clusters (Figure 4.1C).

Histological features of apoptosis included shrinkage and diffuse bright pink discolouration (hypereosinophilia) of the cytoplasm, often leading to an optically empty halo separating the apoptotic cell from the adjacent cells, and concurrent shrinkage (pyknosis) and fragmentation (karyorrhexis) of the nucleus (Figure 4.1C).

Regeneration was detected as an increase in the numbers of mitotic figures not exclusively restricted to the basal layer (as expected in a normal epithelium) but scattered throughout the full thickness of the respiratory mucosa (Figure 4.1D), on occasion associated with subjectively increased numbers of epithelial layers (epithelial hyperplasia). In some rare instances, few, mostly individualised or grouped in very small clusters, epithelial cells displayed features typical of squamous cells, however in the absence of any obvious keratinisation.

Representative pictures of tracheal explants recapitulating the most relevant histological features are shown in Figure 4.1.

Figure 4.1 Histopathological features of EIV infected explants.

Representative pictures recapitulating the major changes observed in EIV infected explants (H&E). A mock infected explant exhibits a pseudostratified respiratory epithelium with an intact outer layer of tall columnar ciliated cells (black arrows) (A) as opposed to an EIV infected explant where a diffuse loss of the ciliated layer is accompanied by diffuse attenuation of the epithelium (black arrows) (B). In addition, scattered apoptotic profiles, either identified as individual cells (black asterisk) or clustered in small groups (white asterisks) are noticed in EIV infected explants and characterised by a small hyperchromatic (pyknotic) nucleus and shrunken hypereosinophilic cytoplasm surrounded by a clear halo. Detail from the previous pictures (C). Occasional mitoses (white arrow) are seen as sign of regeneration (D).

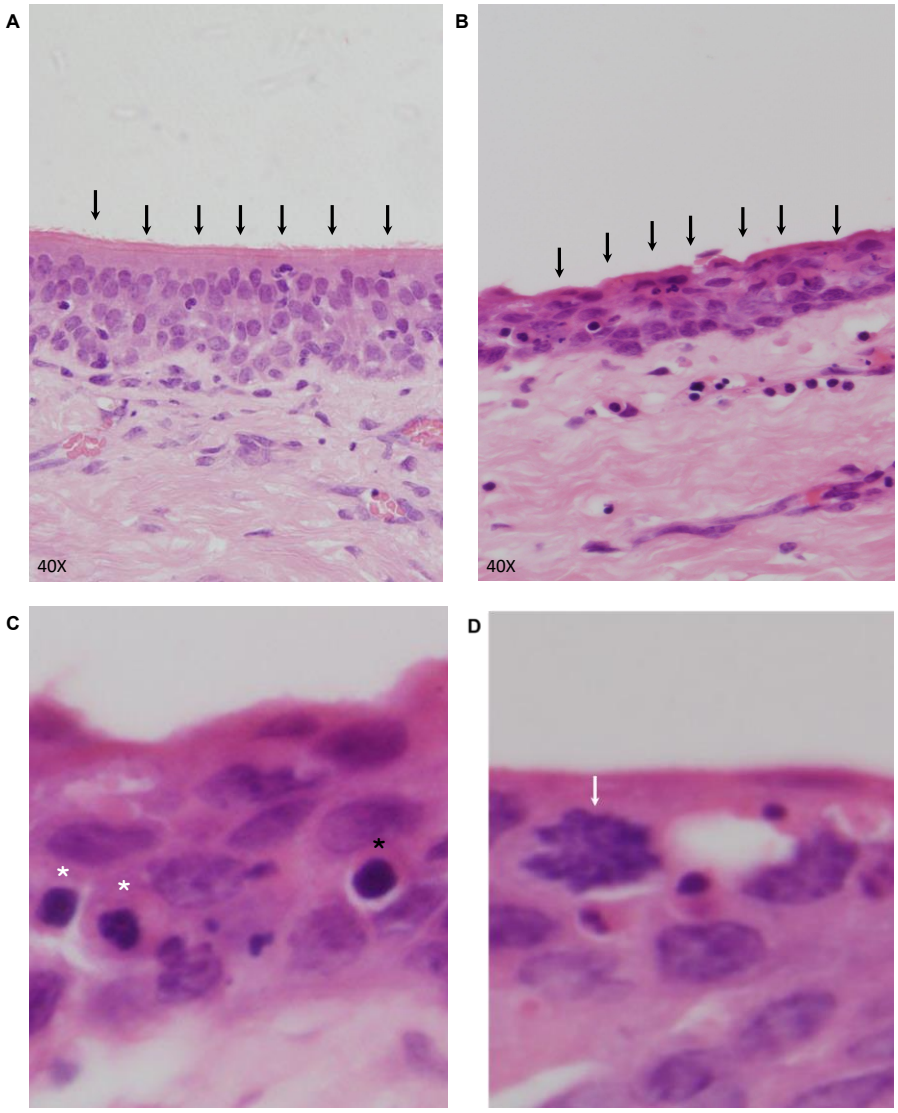

4.2 Description of immunohistochemical changes

As part of the histopathological characterisation and particularly to make a reliable correlation between the histopathological changes and the presence of the virus in the examined samples, immunohistochemistry for the viral nucleoprotein (NP) was performed. As expected, NP displayed an irregularly dotted pattern, mostly exclusively restricted to the nuclei within the respiratory epithelial compartment in superficial and more basal cells. Exceedingly rare cells with brown-stained cytoplasm interpreted as macrophages were observed scattered throughout the epithelium and in the submucosa (Figure 4.2).

Figure 44.2 Representative pictures of NP.
NP staining was characterised by an irregularly dotted pattern, almost exclusively restricted to the nuclei (black arrows) within the respiratory epithelial epithelium of infected explants. Exceedingly rare macrophages exhibited a faint cytoplasmic positivity (asterisk).

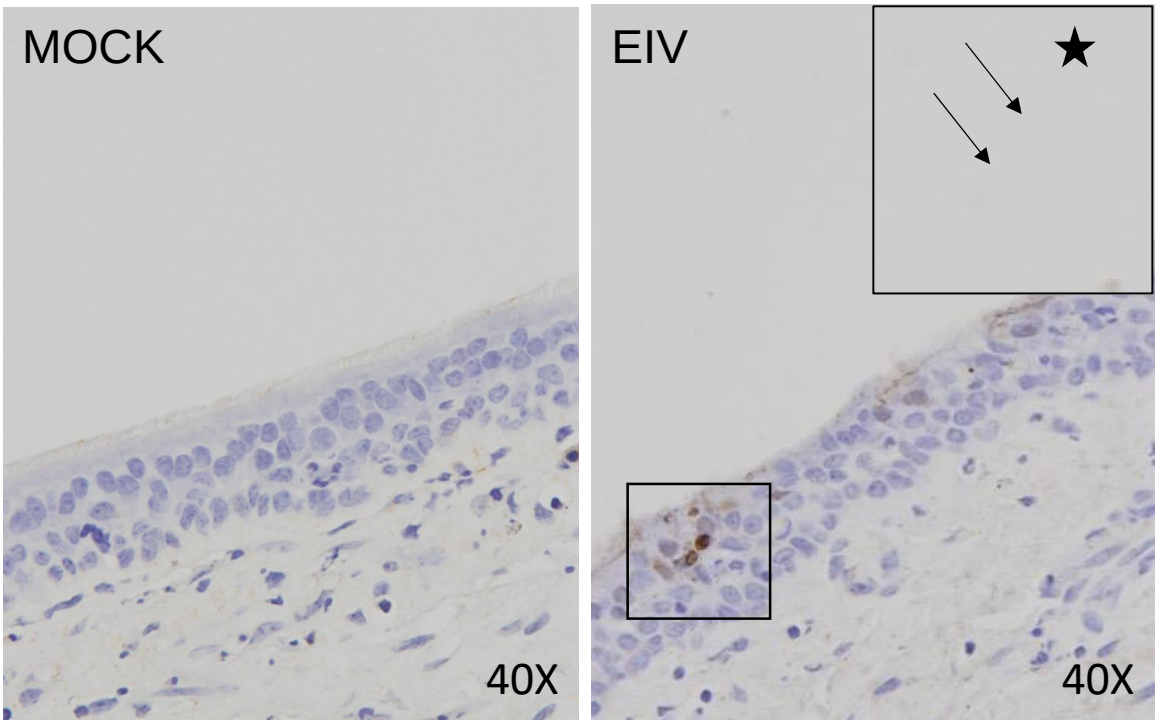

After demonstrating the presence of the virus in the tracheal respiratory epithelium of infected explants and the absence of the virus in the mock infected ones, the subsequent steps were the assessment of virus-induced apoptosis by cleaved caspase 3 (CC3).
CC3 is one of the executioners of apoptosis and once its cleavage is activated, the cell unavoidably undergoes apoptosis which is a form of programmed cell death either normally found in certain

tissues or on occasion triggered by pathological processes such a viral infection (Kumar, Abbas, & C, 2015).

CC3 demonstrated a strong nuclear and nuclear/cytoplasmic pattern of staining in cells committed to death (sporadic apoptotic cells) and in heavily degenerate to disrupted and fragmented cells (interpreted as apoptotic bodies) (Figure 4.3). CC3 revealed to be a particularly useful tool to detected early apoptosis.

Figure 4.3 Representative pictures of CC3.

CC3 staining was characterised by a nuclear and nuclear/cytoplasmic pattern of staining in cells committed to death (black arrow) and in heavily degenerate to disrupted and fragmented cells (apoptotic bodies) (white arrow) respectively.

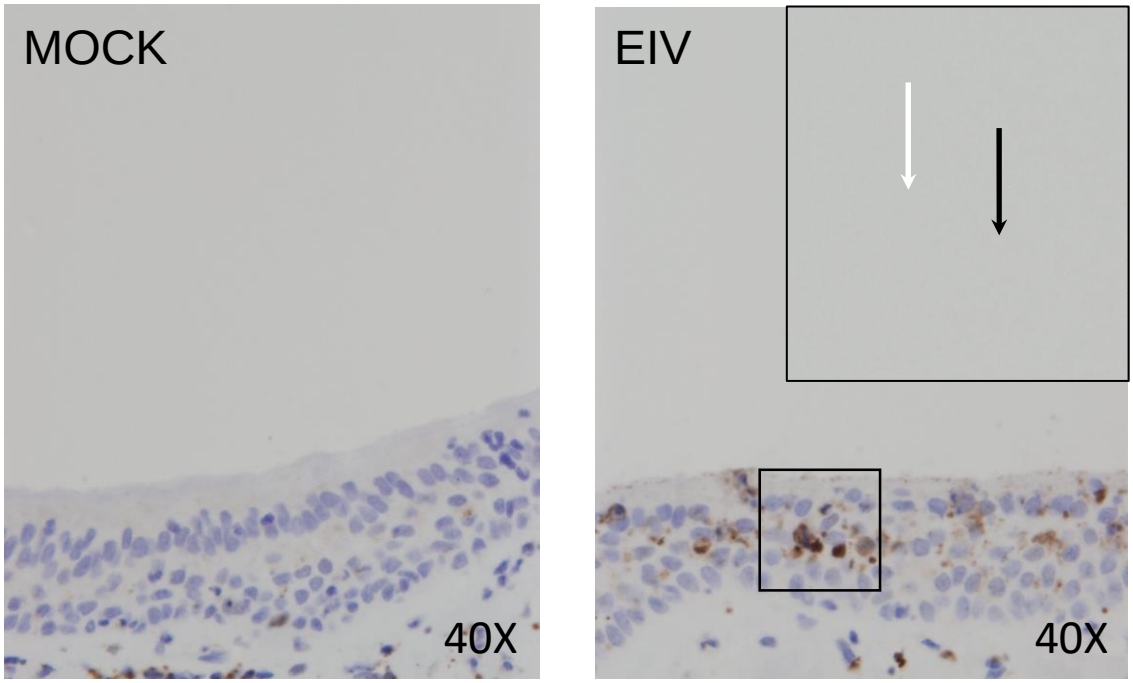

Finally, the regenerative processes were analysed in terms of Ki67 expression.

Ki67 is a very well-known proliferation marker present in all the active phases of the cell cycle (G1, S, G2, and mitosis) and largely used as an indicator of the proliferative potential in normal tissues or tumours (Maglennon, et al., 2008). The marker is characterised by a staining which is exclusively nuclear and exhibits a gradient of expression (from very faint to very strong).

Representative IHC pictures of Ki67 staining are shown in Figure 4.4.

Figure 4.4 Representative pictures of Ki67.

Ki67 expression was exclusively nuclear with a gradient of expression (from very faint to very strong). Positive nuclei were restricted to the basal layer in mock explant (as expected), whereas they were scattered throughout the full mucosal thickness in EIV infected explants.

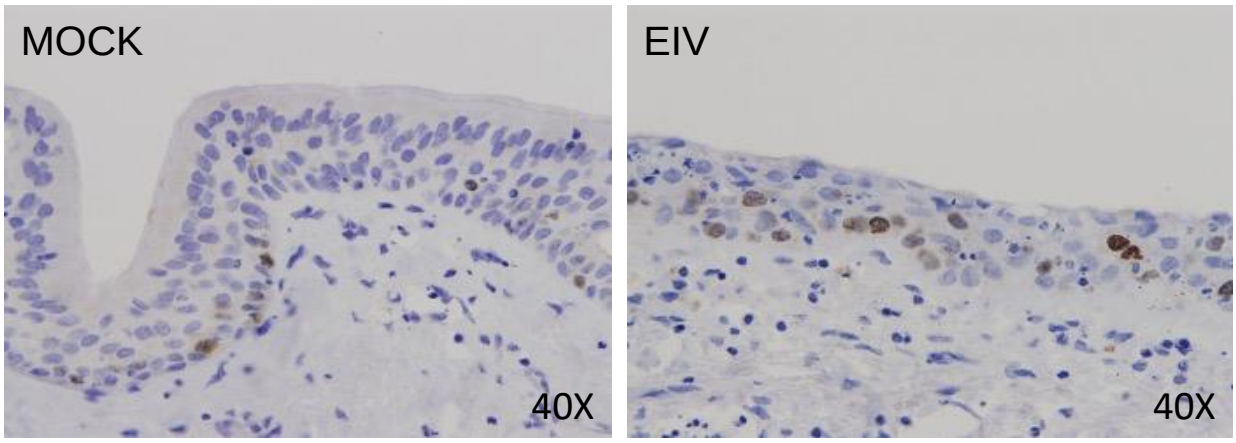

4.3 Semiquantitative analysis – Immunohistochemistry

Following the preliminary histopathological evaluation, my effort was primarily to confirm differences between mock and infected explants not only demonstrating the presence/absence of the afore listed immunohistochemical markers, but also trying to score them with the goal of quantifying pathological changes in EIV infected explants.

4.3.1 NP

In all the samples with obvious histopathological changes, NP signal was clearly observed, confirming EIV infection as the underlying cause for the observed tissue damage; the opposite was true for the mock, where the tissue was within normal limits in the absence of the viral antigen (as expected) and the very minimal alterations observed – particularly at the edges of the slices – were attributed to handling procedures, possibly exacerbated by adaptation to culture conditions.
The semiquantitative scoring of NP was of binary nature (nominal type) and the samples were simply assigned to one out of two categories (presence or absence of the viral antigen) in the absence of any reference to the quantity of viral antigen detected.
NP semiquantitative scoring is reported in Table 4.1.

4.3.2 CC3

The evaluation of apoptosis in terms of CC3 expression was performed following an ordinal approach (Gibson-Corley, et al., 2013; Meyerholz & Beck, 2018).
CC3 was categorised as reported in material and methods and in Table 4.1.
Starting from 2 dpi, an obvious increase in CC3 expression was evident in explants infected with EIV and persisted until 4 dpi.
At 5 dpi the semiquantitative expression of CC3 was within the range seen in mock infected explants.

4.3.3 Ki67

In contrast to what performed for NP and CC3, Ki67 was counted at the microscope in terms of positive nuclei over a total of 100 nuclei at high power magnification (400x), with the positive nuclei considered exclusively restricted to epithelial cells.

The count was performed one single time by me as a single operator to eventually obtain a percentage of nuclear positivity.

Evidence of increased proliferation was present at 2 dpi, however reaching its peak of expression at 4 dpi.

The results of Ki67 manual count are summarised in Table 4.1.

Table 4.1 Semiquantitative analysis of NP, CC3, and manual count of Ki67 (nuclear percentage).

For NP, the presence (p) or absence (a) of the antigen was assessed. For CC3, a subjective (semiquantitative) score was assigned to each explant (0 = no signal; 0,5 = scattered positive cells; 1 = patchy aggregates in up to 10%; 2 = patchy aggregates in more than 10%). For Ki67, the numbers of positive nuclei (regardless of their grading intensity) were counted on a total of 100 epithelial nuclei to generate a percentage. All the above-mentioned analyses were made by a single operator. Missing samples are reported as //. M: mock; EIV: equine influenza virus (suffix numbers 1 or 2 represent replicate number).

group	NP	CC3	Ki67(%)
day 1 M1	a	0,5	2
day 2 M1	a	0,5	5
day 2 M2	a	1	7
day 3 M1	a	0	3
day 3 M2	a	0	2
day 4 M1	a	1	5
day 5 M1	a	0,5	1
day 5 M2	a	0,5	1
day 1 EIV1	a	1	6
day 1 EIV2	a	0,5	1
day 2 EIV1	a	1	4
day 2 EIV2	p	2	8
day 3 EIV1	p	2	10
day 3 EIV2	a	0,5	1
day 4 EIV1	p	2	26
day 4 EIV2	p	1	9
day 5 EIV1	p	//	4
day 5 EIV2	p	0,5	1

4.4 Semiquantitative analysis – Histopathology

The pathological changes taken into account for histopathological evaluation included cellular loss (loss of ciliated epithelium and/or goblet cells), epithelial degeneration (in terms of epithelial attenuation and/or increased numbers of individualised or small clusters of hypereosinophilic apoptotic cells with pyknotic nuclei), and obvious regenerative processes (increased number of epithelial cells and/or epithelial layers and/or increased mitotic rate) and were exclusively evaluated within the respiratory epithelium.

The semiquantitative analysis of pathological changes was performed as a binary analysis (Gibson-Corley, Olivier, & Meyerholz, 2013) for the following 4 categories:

1) cellular loss (loss of ciliated epithelium and/or goblet cells);
2) epithelial attenuation;
3) apoptosis;
4) increased number of mitotic figures.

The mock infected explants did not show any obvious pathological/degenerative or regenerative changes as expected with the only exception of a single mock infected explant at 5 dpi (identified as day 5 M2 in Table 4.2) where few cells featuring apoptosis were detected.

In the greatest proportion of the examined samples, the morphology at the edges of the sections was (not surprisingly) poorer than in the central areas of the explants likely as a consequence of sampling/crash artefact (possibly also exacerbated by adaptation to culture conditions).

Degenerative and regenerative changes were appreciable in explants infected with EIV as early as 1 dpi. However, for all the 4 categories considered (cellular loss, cellular attenuation, apoptosis, and mitosis), I was unable to grade them. For this reason, the simple presence or absence (binary type of analysis) of the above-listed features was reported.

With regard to regenerative processes, mitotic figures were evident in both mock and EIV infected explants, however appeared to be exclusively restricted to basal layer in the former and scattered also throughout the suprabasal layer in the latter.

Results of histopathological scoring are summarised in Table 4.2.

Table 4.2 Qualitative analysis of histopathological changes.

The following categories, including cellular/cilia loss, attenuation, apoptosis, and increased mitotic figures, were assessed for each sample in terms of presence (p) or absence (a) of each feature. Apoptosis was detectable as early as 1 dpi in infected samples to then disappear from 4 dpi onwards. Mitotic figures were evident in both mock and EIV infected explants; however, in mock explants the mitotic figures were restricted to basal layer whereas in EIV infected explants they were scattered also throughout the suprabasal layer. Missing samples are reported as //. M: mock; EIV: equine influenza virus (suffix numbers represent replicate number).

day	group	cell/cilia loss	attenuation	apoptosis	mitosis
day 1	M1	a	a	a	//
day 2	M1	a	a	a	p
day 2	M2	a	a	a	//
day 3	M1	a	a	a	p
day 3	M2	a	a	a	//
day 4	M1	a	a	a	p
day 5	M1	a	a	a	p
day 5	M2	a	a	p	//
day 1	EIV1	p	p	p	//
day 1	EIV2	p	p	p	p
day 2	EIV1	p	p	p	p
day 2	EIV2	p	p	p	p
day 3	EIV1	p	p	p	p
day 3	EIV2	p	p	p	p
day 4	EIV1	p	p	a	p
day 4	EIV2	p	p	a	p
day 5	EIV1	p	p	a	p
day 5	EIV2	p	p	a	p

4.5 Development of a quantitative image analysis pipeline

The semiquantitative analysis of histopathological changes and immunohistochemical staining (NP, CC3) and the 'manual' count allowing to calculate a percentage of Ki67 in epithelial cells were clearly demonstrating the presence of changes in tracheal explants imputable to EIV infection. However, all the semiquantitative scores and the Ki67 'manual' count were generated by me as a single operator. In addition, semiquantitative analysis for NP and histopathological changes was only possible in terms of binary analysis (Gibson-Corley, Olivier, & Meyerholz, 2013). For this reason, in light of the ultimate scope of my thesis to develop an unbiased method to quantify pathological changes, I decided to use image analysis software to properly quantify the immunohistochemical markers and then to attempt a quantification of histopathological changes.

4.5.1 NP quantification

NP demonstrated its presence in explants infected with EIV starting from 2 dpi to progressively decrease up to 5 dpi where a small amount of signal was however still appreciable in contrast to mock infected explants where no pixels were seen (Figure 4.6A).

A statistically significant difference ($p=0.024$) between mock and EIV infected explants was seen at 3 and 4 dpi respectively (non-parametric Wilcoxon Mann Whitney test) (Figure 4.6B).

4.5.2 CC3 quantification

CC3 showed a peak of expression at 2 dpi in EIV infected explants to afterward progressively decrease until 5 dpi.

A peak of CC3 expression, however below the levels observed in EIV infected explants, was appreciated at 4 dpi in mock infected explants (Figure 4.7A).

Statistically significant ($p=0.024$) and highly significant ($p=0.005$) differences were seen between mock and EIV infected explants at 1 and 5 dpi and 3 dpi respectively (non-parametric Wilcoxon Mann Whitney test) (Figure 4.7B).

4.5.3 Ki67 quantification

Ki 67 demonstrated to increase in EIV infected explants up to 3 dpi to drop down to mock level at 5 dpi. Two relatively small increases were observed at 2 and 4 dpi in the mock explants, and, similarly to what observed for CC3, attributed to culture conditions. Representative IHC pictures are reported in Figure 4.8A.

Statistically significant ($p=0.045$) differences were detected between mock and EIV infected explants at 3 dpi (non-parametric Wilcoxon Mann Whitney test) (Figure 4.8B).

Figure 4.5 Representative pictures and quantification of NP.

Mock and EIV infected explants, representative pictures at 1, 2, 3, 4, and 5 dpi, 40x magnification(A).

NP quantification in mock and EIV infected explants (B). Graphical representation of NP quantification in equine tracheal explants (EIV-infected and mock-infected). A statistically significant difference (p=0.024) between mock and EIV infected explants was seen at 3 and 4 dpi respectively (non-parametric Wilcoxon Mann Whitney test).

A

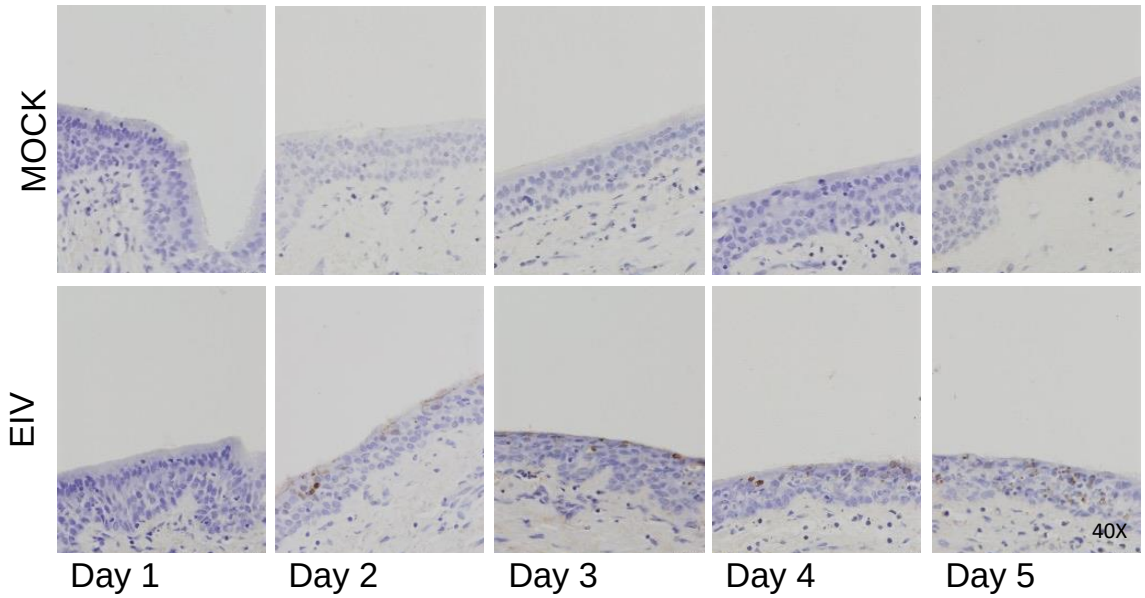

B

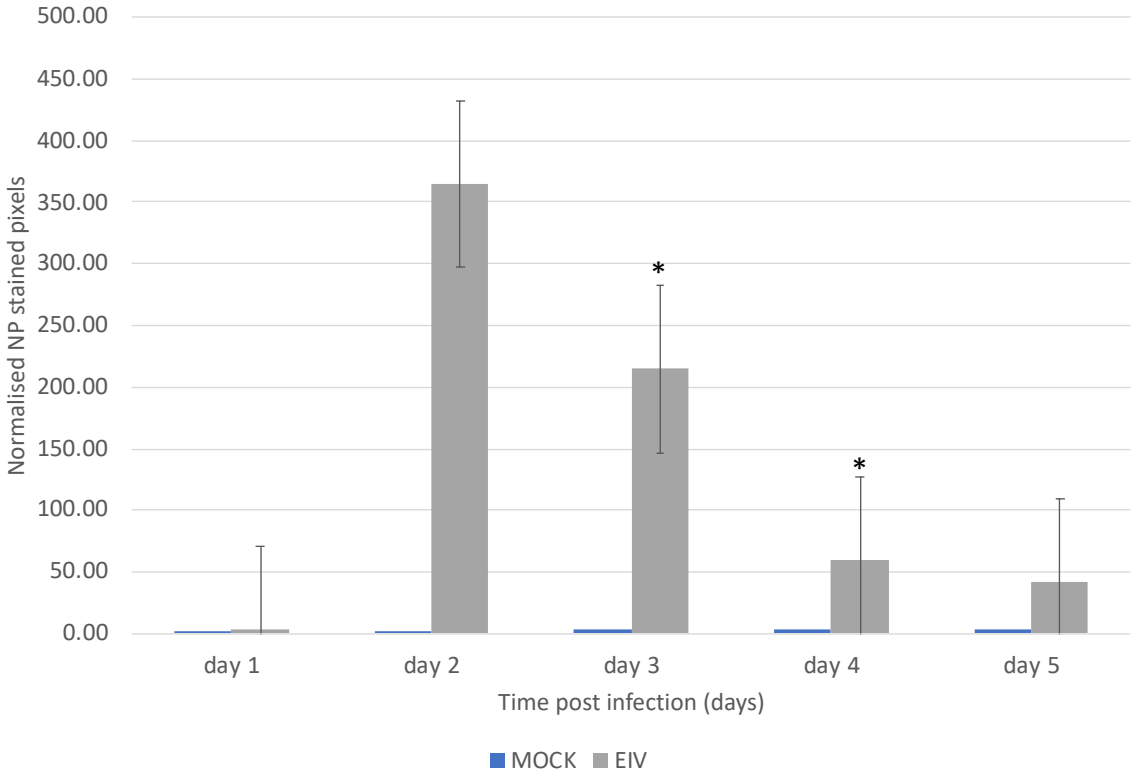

Figure 4.6 Representative pictures and quantification of CC3.

Mock and EIV infected explants, representative pictures at 1, 2, 3, 4, and 5 dpi, 40x magnification (A). CC3 quantification in mock and EIV infected explants (B). Graphical representation of CC3 quantification in equine tracheal explants (EIV-infected and mock-infected). Statistically significant (p=0.024) and highly significant (p=0.005) differences were seen between mock and EIV infected explants at 1 and 5 dpi and 3 dpi respectively (non-parametric Wilcoxon Mann Whitney test).

A

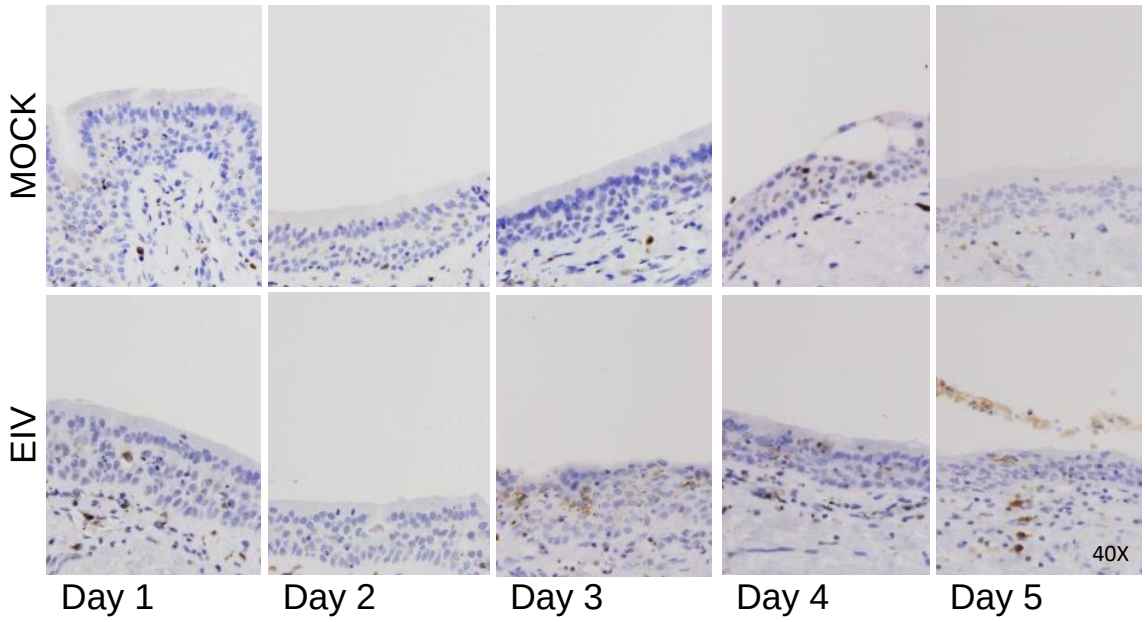

B

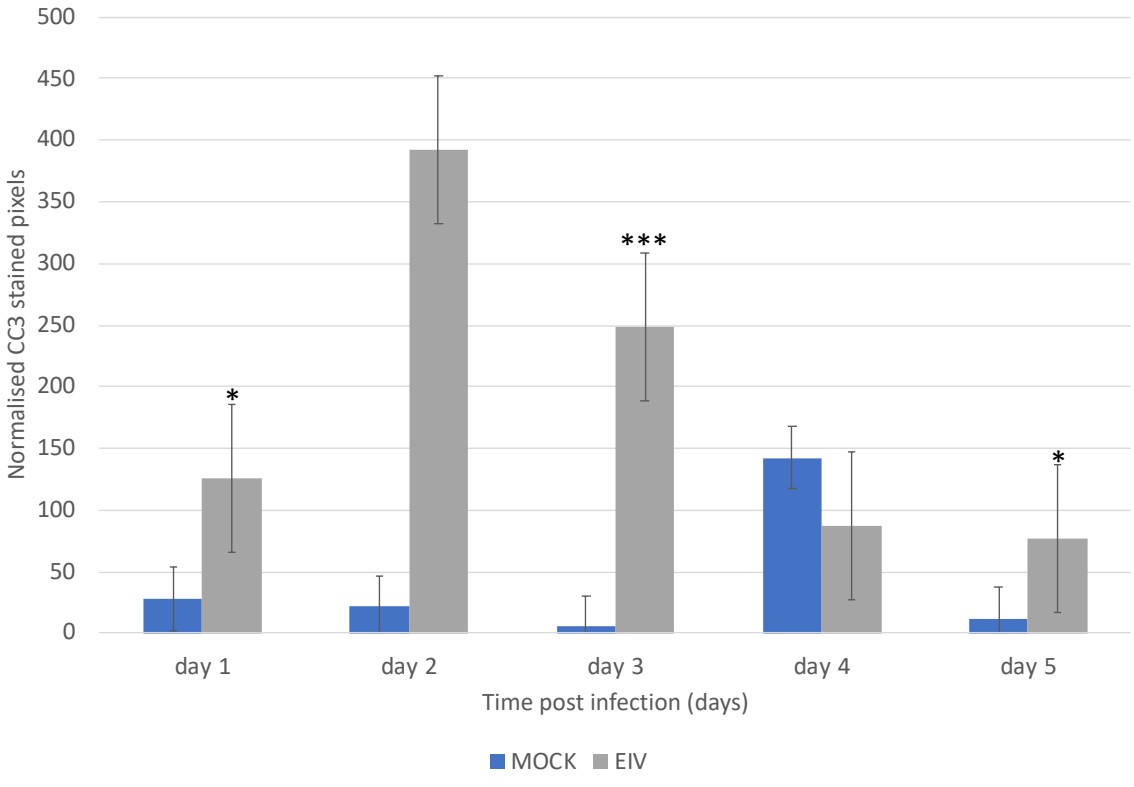

Figure 4.7 Representative pictures and quantification of Ki67.

Mock and EIV infected explants, representative pictures at 1, 2, 3, 4, and 5 dpi, 40x magnification (A). Ki67 quantification in mock and EIV infected explants (B). Graphical representation of Ki67 quantification in equine tracheal explants (EIV-infected and mock-infected). Statistically significant (p=0.045) differences were detected between mock and EIV infected explants at 3 dpi (non-parametric Wilcoxon Mann Whitney test).

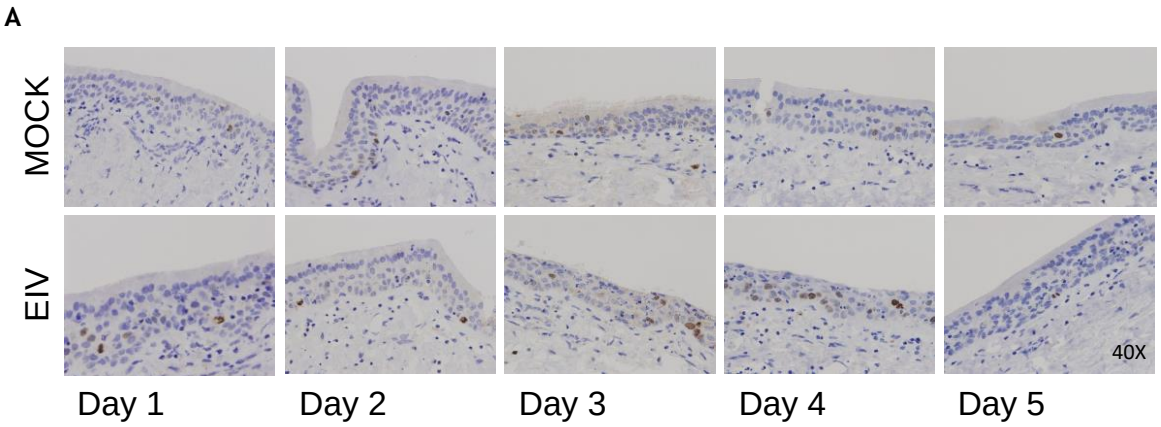

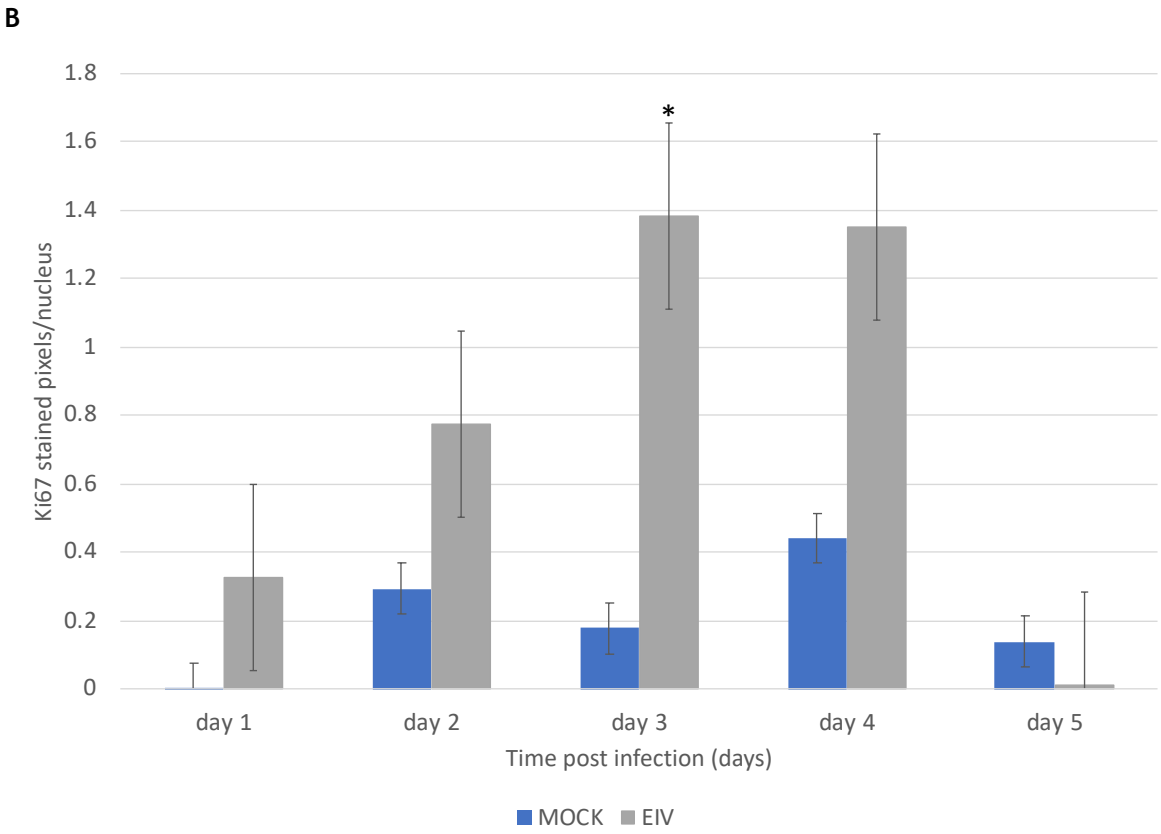

4.6 Interferon-induced GTP-binding protein Mx1 in tracheal explants following EIVs infection

4.6.1 Innate immunity

Interferon-mediated induced Mx proteins are known to play a central role in containing viral infections. Mx proteins (also known as Mx1 and Mx2 in mammals) are broadly expressed with a recognised antiviral activity against DNA and RNA viruses (including influenza viruses, and specifically EIV (Fatima, et al., 2019). Their precise mechanism of action is still under investigation; however, they are very likely to interact with viral NP and possibly also with the polymerase basic protein 2 (PB2) subunit of the RNA-dependent RNA polymerase (RdRp), ultimately halting the formation of viral ribonucleoprotein complexes (vRNPs) (Fatima, et al., 2019).

Adaptive immunity could not be investigated in equine tracheal explants because of the intrinsic *ex-vivo* nature of the EVOC system. However, given the fact that explants recapitulate the most salient features of the upper respiratory airways (including a pseudostratified ciliated epithelium with scattered Goblet cells) together with the very encouraging preliminary results following ImageJ application on IHC stained slides, I decided to quantify changes of innate immunity in response to EIV infection using Mx proteins as a proxy of innate immune activation.

4.6.2 Mx1 immunohistochemistry

Immunohistochemistry for Mx1 was performed on the sections from mock and EIV infected explants previously used. A mouse monoclonal anti-MX1 (clone M143, kindly provided by Georg Kochs) was used at the dilution of 1/200. The steps were as previously reported in material and methods for Ki67.

The pattern of staining as expected was strictly cytoplasmic with a grading of expression from very faint to very intense.

Representative pictures of the staining are shown in Figure 4.9.

Figure 4.8 Representative pictures of Mx1.

Representative pictures of mock and EIV infected explants stained with Mx1. The pattern of staining is strictly cytoplasmic and the signal intensity ranges from faint (mock infected explant) to strong (EIV infected explant).

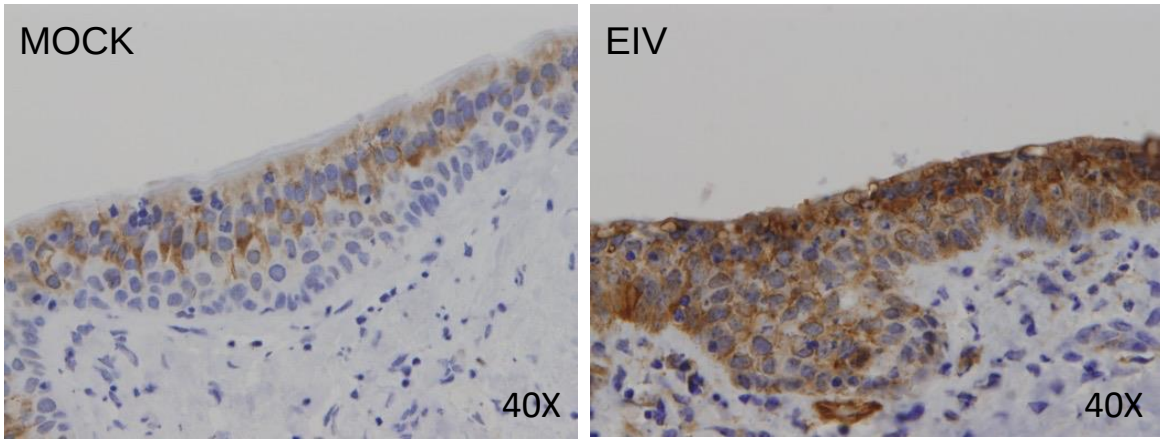

The quantification of Mx1 was then conducted using ImageJ as described for NP and CC3 and the number of stained pixels were quantified in three selected fields at 400x following manual selection and cropping of the epithelium and then normalised by the epithelial length.

Mx1 showed a peak of expression at 4 dpi in EIV infected explants. However, Mx1 expression was also observed in mock infected explants (Figure 4.9), albeit at lower levels.

Statistically significant ($p=0.030$; $p=0.024$) and highly significant ($p=0.002$) differences were seen between mock and EIV infected explants at 3 and 4 dpi (significant) and 5 dpi (highly significant) respectively (non-parametric Wilcoxon Mann Whitney test) (Figure 4.10).

Figure 4.9 Mx1 quantification.

Graphical representation of Mx1 quantification in equine tracheal explants (EIV-infected and mock-infected). Statistically significant (p=0.030; p=0.024) and highly significant (p=0.002) differences were seen between mock and EIV infected explants at 3 and 4 dpi and 5 dpi respectively (non-parametric Wilcoxon Mann Whitney test).

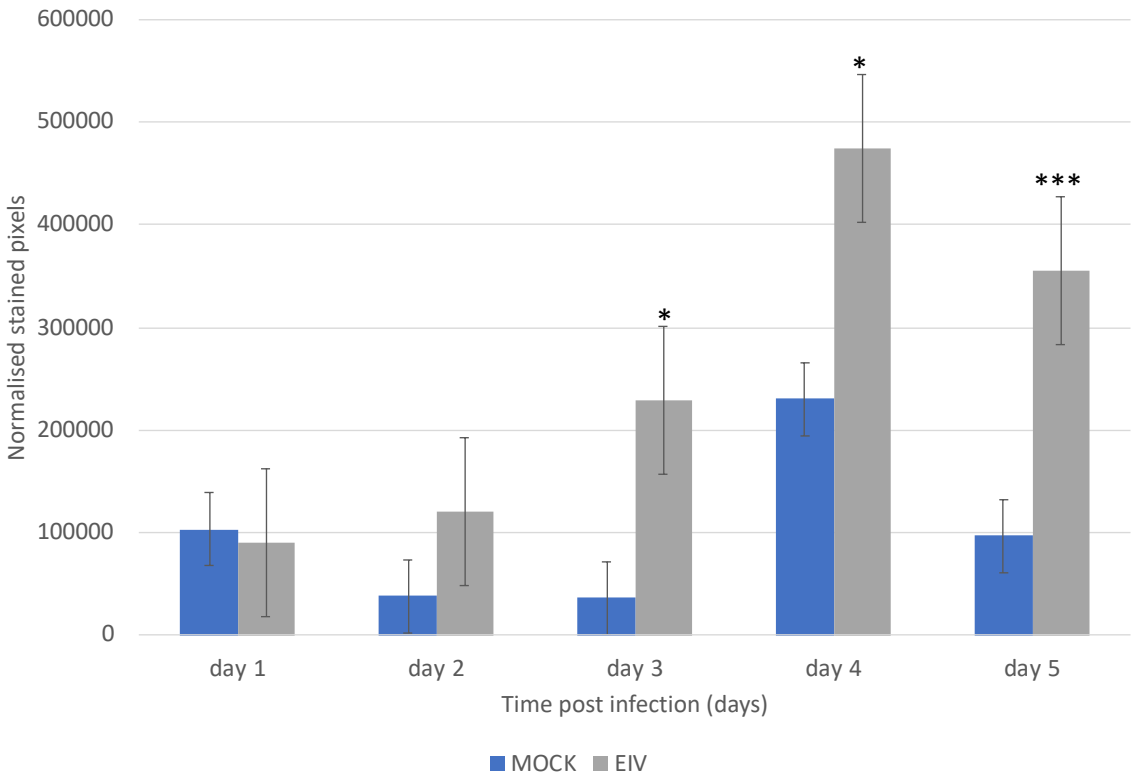

4.7 Quantification of histopathological changes

Given the results obtained with ImageJ on IHC-stained sections and the versatility of the software, I set out to quantify histopathological changes. To this end, all the analysed pictures were processed with ImageJ to extract the number of nuclei and the nuclear area (area covered by the nuclei within respiratory epithelium). The aim behind this approach was to translate in measurements the reduction in cellularity in terms of reduction in the numbers of nucleated cells (less nuclei equal less cells) and to quantitatively describe the nuclear changes accompanying degenerative/regenerative changes in infected explants, including nuclear shrinkage/condensation (variation in nuclear area equals variation in nuclear size/shape).

4.7.1 Number of nuclei

The number of nuclei were obtained from approximately 330 pictures taken for NP, CC3, Ki67, and Mx1 analysis and normalised by the length of the epithelium.

In mock explants a first decrease was observed at 2 dpi followed by a second decrease at 5 dpi (Figure 4.11).

Statistically significant (p=0.024) differences (non-parametric Wilcoxon Mann Whitney test) were seen between mock and EIV infected explants at 4 dpi (Figure 4.11).

Figure 4.10 Quantification of epithelial nuclei.

Graphical representation of nuclei quantification in equine tracheal explants (EIV infected and mock infected). Statistically significant (p=0.024) differences were seen between mock and EIV infected explants at 4 dpi (non-parametric Wilcoxon Mann Whitney test).

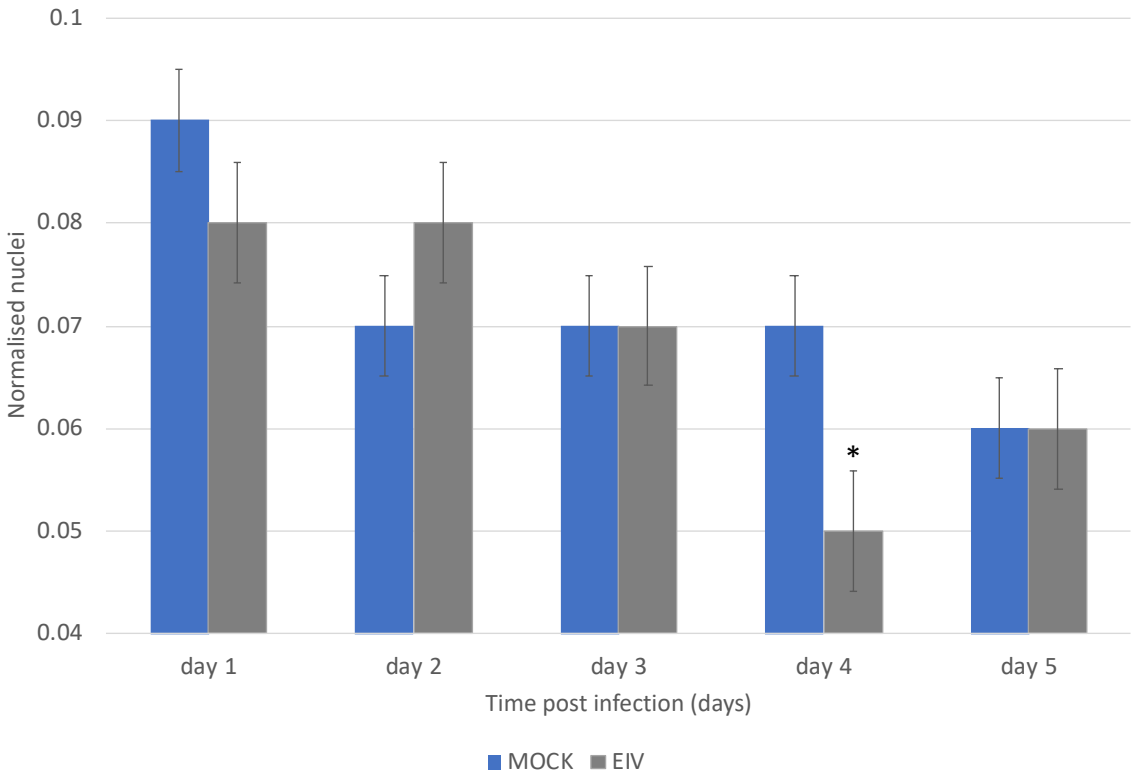

4.7.2 Nuclear area

On the same pictures used for the quantification of the number of nuclei, the area covered by the nuclei was assessed (Figure 4.12).

Statistically significant (p=0.024) differences (non-parametric Wilcoxon Mann Whitney test) were seen between mock and EIV infected explants at 4 dpi (Figure 4.12).

Figure 4.11 Quantification of nuclear area.

Graphical representation of nuclear area quantification in equine tracheal explants (EIV infected and mock infected). Statistically significant (p=0.024) differences were seen between mock and EIV infected explants at 4 dpi (non-parametric Wilcoxon Mann Whitney test).

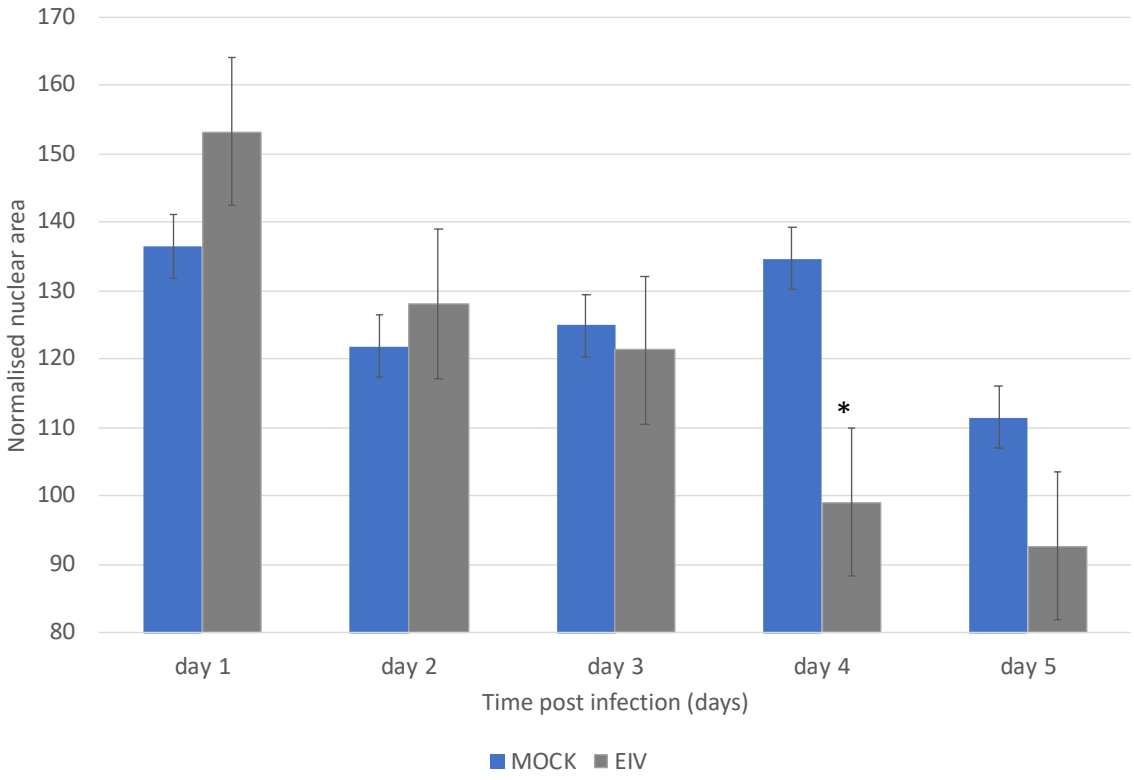

5 Discussion

In this thesis I wanted to explore the possibility to quantify 'pathology' in an unbiased way.
Pathological/histopathological analysis can be applied to a variety of situations from naturally occurring to experimentally induced diseases, but particularly when it comes to experimental infections, the assessment of lesions in terms of presence/absence of morphologic alterations is considered not sufficient per se and the pathologist is specifically called to highlight differences amongst diverse experimental groups, in other words to define the extension (magnitude/severity) of the pathological processes (Grant Maxie & Miller, 2016).
An accurate determination of the severity of the lesions is also more than beneficial in the context of diagnostics, allowing to more reliable prognostication and more appropriate definition of further clinical management/therapeutic schedule if needed. Therefore, the traditional approach of performing a histopathological scoring (or grading) has acquired a key role in the daily routine of pathologists (Treuting & Boyd, 2019). However, the histopathological scoring has a series of unavoidable intrinsic limitations, first of all it only provides a semiquantitative analysis and should be ideally performed in a blind fashion by two independent operators (trained and experienced, possibly also board-certified pathologists) (Shott, 2011). Whether performing a blind analysis is thought to be an essential requisite for an unbiased grading, on the other hand ideally the operator should be fully aware of the experimental set and related objectives and methods in order to produce meaningful data (Treuting & Boyd, 2019). In addition, the repeatability of histopathological grading can be affected by a very broad variety of visual and cognitive biases (e.g. mental noise, diurnal fluctuations, etc) that can't be truly prevented or controlled (La Perle, 2019).
The advent of new digital technologies for image analysis has offered the possibility to overcome the limitations of histopathological scoring and not only provide with meaningful and reproducible data, but also produce data that are further suitable to statistical analysis.
If the role of the pathologist remains crucial for setting up the software and ultimately for interpreting and validating the obtained data, on the other hand the image analysis software allows to convert pathological changes into measurements (e.g. numbers of stained pixels) (Grant Maxie & Miller, 2016).
The only limiting factor of image analysis resides in what precedes the analysis itself, that is all the sampling or lab procedures to obtain the slides submitted for analysis (La Perle, 2019). This, however, in my personal opinion, is likely easy to be kept under control through a rigorous system of standard operating procedures.
Amongst the broad selection of software available, I decided to start with a freely downloadable image analysis program (ImageJ) developed at the National Institutes of Health and the Laboratory for Optical and Computational Instrumentation (LOCI, University of Wisconsin) which has been firstly released in 1997 (Schneider, Rasband, & Eliceiri, 2012) (Collins, 2007).
I tested ImageJ on a well characterised *ex vivo* organ culture (EVOC) system such as equine tracheal explants, largely used over the past years to investigate EIV infection dynamics.

5.1 Semiquantitative analysis – Histopathology

Before starting with any proper quantification, I wanted to assess the good quality of the selected system. For this reason, I have firstly attempted a very traditional approach focusing on the detection of morphological changes induced upon viral infection.

What appeared obvious was that there were morphological changes in infected explants likely to be attributed to EIV infection. Overall, the lesions were consistent with cellular loss (in term of both loss of the ciliated epithelium and Goblet cells), epithelial degeneration (attenuation/apoptosis), and epithelial regeneration.

The most obvious microscopic change was the thinning of the respiratory epithelium in the infected samples likely resulting from superficial epithelial sloughing.

Epithelial degeneration was characterised by attenuation of the suprabasal layer of the respiratory epithelium and increase in the number of apoptotic cells, either recognised as individual apoptotic cells or grouped in small apoptotic clusters (apoptotic bodies).

Regeneration in the infected explants was first of all detected as an increase in mitoses throughout the full thickness of the respiratory mucosa (instead of being only restricted to the basal compartment), which in turn was occasionally characterised by epithelial hyperplasia. In very rare instances, evidence of few, very small clusters of epithelial cells displaying features potentially consistent with squamous cells (squamous metaplasia) were seen. Squamous metaplasia (and more in general metaplasia) is a process seen as a consequence of a broad variety of pathological condition (ranging from longstanding inflammation to vitamin A deficiency to repeated exposure to injuries) (Miller & Zachary, 2017). In the respiratory epithelium, the change to a squamous phenotype is seen in conjunction with loss of the superficial epithelium and Goblet cells and very likely represents an attempt to prevent secondary infections otherwise facilitated by the absence of a functional mucociliary clearance (Miller & Zachary, 2017). In the context of tracheal explants, I interpreted this change as an accompanying feature of regeneration, however of very minimal entity. No obvious concurrent epithelial loss/ulceration was appreciated.

The histopathological phenotype of EIV infected explants was remarkably consistent to what had been described in tracheas of horses experimentally infected with EIV (Muranaka, et al., 2012). The main difference observed regarded the presence of inflammation as expected considering the intrinsic *ex-vivo* nature of the EVOC system.

Whether the loss of ciliated epithelial cells and Goblet cells was evident in both the *ex-vivo* and the *in-vivo* experimental models and in both represented the earliest sign attributable to EIV infection (1 dpi in explants as opposed to 2 dpi in experimentally infected horses), the more exquisitely regenerative processes (and particularly epithelial hyperplasia/squamous metaplasia) were more obvious in the *in-vivo* model and not surprisingly given the fact that the experimental infection had been studied over the course of a longer time frame (14 days) compared to the relatively limited duration (5 days) of the *ex-vivo* infection.

In terms of epithelial degeneration, the vacuolar changes described as a prominent feature in the tracheas of experimentally infected horses were not as obvious in the respiratory epithelium of infected explants, albeit an increased number of apoptotic cells (both as increased number of individual apoptotic cells or evidence of small foci of apoptotic cells/apoptotic bodies) was

appreciable in the latter, not unfrequently in combination with evidence of epithelial sloughing and marked attenuation. The underlying reason for this difference amongst *ex-vivo* and *in-vivo* models is not entirely clear at this stage, however, whether the value of the EVOC system is undeniable in terms of recapitulating the most salient features of a trachea and also in terms of complying the 3Rs system, it has to be stressed that only a very small (0.5x0.5 cm) fragment of tissue is made available for examination, whereas in experimentally infected horses the amount of tissue available is greater with the possibility to get multiple transmural and circumferential sections of trachea. Additionally, as demonstrated by Muranaka et al. (2012), it has to be pointed out that changes might differ in relation to the level of sampling (e.g. cranial vs caudal trachea; in experimentally infected horses tracheitis appeared to be more severe in the caudal portion of the trachea) (Muranaka, et al., 2012). This particular piece of information (site of collection) was missing for the explants used in this research project.

5.2 Semiquantitative analysis – Immunohistochemistry

As part of the histopathological characterisation, I decided to perform immunohistochemistry as an ancillary test to investigate viral infection/spread (NP), apoptosis (CC3), and regenerative changes (Ki67) in equine tracheal explants.
Immunohistochemistry technique was favoured instead of immunofluorescence given the longer preservation of the immunostained slides granted by the use of a chromogen (DAB) rather than a fluorochrome. In this way, I could analyse the slides over the course of my research project without compromising the quality of the staining. For each marker studied, freshly cut slices were stained immediately after sectioning and subsequently the stained slides were carefully stored in a dedicated histology cabinet to prevent any damage/deterioration due to light exposure and/or inappropriate handling.

The first goal was to investigate by immunohistochemistry the presence of EIV in infected explants and therefore to correlate the evidence of pathological changes to the effective presence of the virus.
For this purpose, I employed an antibody directed against NP to detect viral antigen, similarly to what described by Gonzalez, et al. (2014) in canine explants.
NP is primarily implicated in nuclear targeting and plays its role when the virus has already entered into the cell, for this reason, it suits best to investigate the spread of the infection in terms of viral replication. Another useful antibody, however, that had not been tested in my research project, but had been used on equine tracheas of experimentally infected horses (Muranaka, et al., 2012), is hemagglutinin (HA) which facilitates viral attachment to target cells and for this reason would be useful used in conjunction with NP to give a thorough overview of EIV infection dynamics.
NP was almost exclusively restricted to the epithelial compartment and its pattern of expression essentially consistent with what showed by Gonzalez in canine tracheal explants with evidence of positive signal in both superficial and more basal cells (Gonzalez, et al., 2014). Exceedingly rare, individual cells scattered in the epithelium and lamina propria/submucosa displayed a brown, on

occasion irregularly granular cytoplasm, however in a very restricted number of infected explants. Whether their significance was not definitely determined, however taking into account the evidence of immunostained macrophages in experimentally infected horses in the lamina propria/submucosa at different levels of the respiratory tracts (including the trachea) (Muranaka, et al., 2012), it can be tentatively speculated that these 'brown' cells may represent macrophages infected by EIV or antigen presenting cells or alternatively macrophages exerting their scavenging function (phagocytosing fragments of disrupted infected epithelial cells). As a possible alternative explanation, also haemosiderin-laden macrophages entrapped at the moment of explant collection (and thus to be interpreted as an incidental finding) should need to be considered given the impossibility to distinguish between antigen stained by chromogen and pigment (haemosiderin), without an appropriate histostaining (Perls Prussian Blue for iron). Additionally, specific IHC markers (e.g. IBA-1) might also need to be considered to rule in/rule out the histiocytic nature of cells with cytoplasmic staining.

Given the presence of a substantially increased number of apoptotic cells in EIV infected explants, I decided to apply the immunohistochemistry technique to better characterise the process.

Apoptosis is an extremely tightly regulated way of programmed cell death which may be seen both as a physiologically occurring process (during development) or as a consequence of irrevocable cellular damage (Cellular Responses to Stress and Toxic Insults: Adaptation, Injury, and Death, 2005).

The process is morphologically (histologically) appreciable as a cellular shrinkage and nuclear condensation and fragmentation, ultimately leading to the formation of the so-called 'apoptotic bodies' which in turn are easily detected and removed by macrophages (Kumar, Abbas, & C, 2015).

Other mechanisms of cell death besides apoptosis would include necrosis (oncotic necrosis), necroptosis (programmed necrosis), and pyroptosis. Whether necrosis mostly accounts for hypoxic injury as the major underlying triggering factor (Miller & Zachary, 2017) and pyroptosis has been prominently associated with bacterial infection (Cellular Responses to Stress and Toxic Insults: Adaptation, Injury, and Death, 2005), and thus both processes seems to be not really relevant in viral infections, necroptosis may be triggered by RNA and DNA viruses.

According to Nogusa et al. (2016), apoptosis and necroptosis are both processes evoked by influenza A virus both in vitro (cell cultures) and in vivo (murine model).

For my research I investigated apoptotic changes by means of CC3. The decision was made on a very practical basis (availability of the antibody) but supported also by the observed changes which were morphologically consistent with apoptosis rather than necroptosis (cellular shrinkage/nuclear condensation as main feature of apoptosis as opposed to cellular swelling as main feature of necroptosis).

Regardless of the pathway of activation (intrinsic or extrinsic), caspase-3 represents one of the executioner caspases and once cleaved the cell is irremediably committed to die (Kumar, Abbas, & C, 2015).

Therefore, CC3 was particularly beneficial in my hands to detect early stages of apoptosis, otherwise microscopically unapparent.

Finally, the regenerative processes were analysed in terms of Ki67 expression.

Ki67 is a nuclear protein that had been largely investigated and used as a prognostication factor for tumours in both human and veterinary medicine (Maglennon, et al., 2008). It accounts for an expression strictly restricted to the nucleus, ranging from a very faint to a very strong brown staining, and is expressed in cycling cells in all the active phases (Vascellari, et al., 2012). Whereas the Ki67 was exclusively located to the basal layer in the mock explants - as expected since the basal layer typically represents the reserve layer in normal epithelia - its distribution became more spread throughout the mucosal thickness in the infected explants and interpreted as a sign of active regeneration.

The subsequent step, before challenging a proper quantitative analysis, was to perform a 'traditional' histopathological scoring of all the immunohistochemical markers and the pathological changes.
I opted for a blind analysis performed by me as a single operator for all the markers investigated.
The semiquantitative scoring of NP was of binary nature (nominal type) (Gibson-Corley, Olivier, & Meyerholz, 2013). Briefly, the presence/absence of the stained viral antigen lacking any reference of its quantity was recorded by me.
NP was evident by eye in EIV infected explants as early as 2 dpi in contrast to what seen by Gonzalez et al. in canine tracheal explants where the virus was evident as early as 1 dpi (Gonzalez, et al., 2014). Interestingly, viral antigen (although stained by a monoclonal antibody directed against HA) was evident as early as 1 dpi and in large numbers of epithelial cells also in tracheas from experimentally infected horses, and still appreciated, although in very small numbers of cells, in horses euthanised at 14 dpi (Muranaka, et al., 2012).

The evaluation of CC3 followed an ordinal approach (Gibson-Corley, Olivier, & Meyerholz, 2013) and the samples were assigned to different categories based on the amounts of antigen subjectively estimated by me (as a single operator).
From 2 dpi an obvious expression of CC3 was evident in explants infected with EIV persisting until 4 dpi. At 5 dpi the level of CC3 appeared by eye to be within the range seen in mock infected explants. Also, in the case of CC3 expression, similarly to what reported for NP, the timing of expression appeared to be different from what observed by Gonzalez, et al. (2014) where the expression of CC3 was evident as early as 1 dpi to gradually increase over the course of the experiment.

In contrast to what performed for NP and CC3, for Ki67 I decided to perform a count at the microscope in terms of number of positive nuclei over a total of 100 nuclei at high power magnification (400x), exclusively within the respiratory epithelium. This is the standard way to evaluate Ki67 in clinical diagnostic settings (e.g., proliferative index in tumours) (Maglennon, et al., 2008) and essentially all the positive nuclei regardless their staining intensity were counted.
The count was performed one single time by me, and a percentage of nuclear positivity obtained.
Proliferation appeared to be increased at 2 dpi, however reaching its peak of expression at 4 dpi.
Overall, as per semiquantitive analysis of CC3 and 'manual' count of Ki67, regenerative processes appeared to occur concurrently to apoptotic processes.

A binary type of analysis (Gibson-Corley, Olivier, & Meyerholz, 2013) was also applied to investigate pathological changes, including cellular loss (loss of ciliated epithelium and/or goblet cells), epithelial attenuation, apoptosis, and increased number of mitotic figures.

The mock infected explants didn't reveal any obvious pathological and/or degenerative/regenerative changes as expected with the only exception of a single mock infected explant at 5 dpi where few cells featuring apoptosis were detected. The reason for this was not entirely clear, however several hypotheses may be speculated, including the presence of a previous abnormality while the animal was still alive or alteration due to sample handling at the moment of explant collection. Given the absence of any obvious bacterial or fungal agent, contamination of the sample was considered unlikely, although couldn't be completely ruled out. Overall, taking into account that tracheal explants can be cultured for up to 7 days in the absence of any obvious pathological or physiological (demonstrated via bead assay) change (Gonzalez, et al., 2014), the evidence of apoptotic cells in one single mock sample was interpreted as an incidental finding and of negligible importance in the overall scheme of this experiment.

Degenerative and regenerative changes were appreciable in explants infected with EIV as early as 1 dpi and appeared to be earlier than what seen by Gonzalez et al. (2014)where 3 dpi was the critical timepoint for degeneration.

In the *in-vivo* experimental settings, the degenerative changes were evident at 1 dpi in terms of mild epithelial necrosis/degeneration and mild lymphocytic infiltration to include also cellular loss (ciliated cells and Goblet cells) and become more marked starting from 3 dpi (Muranaka, et al., 2012). Regeneration included epithelial hyperplasia and squamous metaplasia and was evident as a mild change at 2 dpi to become more marked at 14 dpi (Muranaka, et al., 2012).

5.3 Quantitative analysis - Immunohistochemistry

The semiquantitative analysis of histopathological changes and immunohistochemical staining (NP, CC3) and the 'manual' count allowing to calculate a percentage of Ki67 in epithelial cells were really encouraging, pointing to the presence of changes in tracheal explants likely imputable to EIV infection. However, for NP and the pathological changes only a binary type of analysis was possible and all the semiquantitative scores and the Ki67 'manual' count were generated by me as a unique operator.

Particularly with regard to this point, the potential bias inherent to the impossibility for a second revision (performed by a second independent operator) at least partially invalidated the quality of the preliminary, very encouraging results and strongly reinforced the necessity for a proper quantification with the ultimate aim of developing an unbiased methodology to quantify pathological changes that would be ideally applicable either to experimental and/or diagnostic settings.

Daniel Goldfarb provided me the training in how to use ImageJ and developed specific macros for NP, CC3 and Ki67.

NP quantification demonstrated the presence of a peak of expression at 2 dpi in explants infected with EIV, with a statistically significant difference between mock and infected explants at 2 and 3 dpi, to progressively decrease at 5 dpi where a small amount of signal was however still appreciable when compared to mock explants.
The NP quantification strongly supported the timing as per previous semiquantitative analysis but in addition provided also a picture of the trend of infection in terms of amount of viral antigen where its progressive decrease over time may suggest an attempt of the respiratory epithelium to clear up the infection. As mentioned before, there is a discrepancy in the timing of expression of NP in equine explants when compared to canine explants (Gonzalez, et al., 2014). Overall, this difference observed in the 2 EVOC systems may be not surprisingly imputable to different susceptibility to EIV infection depending on background species (canine vs equine).

Quantitative analysis indicated a peak of expression of CC3 at 2 dpi in EIV infected explants with a significant difference and a highly significant difference between mock and infected explants at 1 and 5 (significant) dpi and 4 dpi (highly significant) respectively, to afterward progressively decrease until 5 dpi.
A peak of CC3 expression, although below the levels observed in EIV infected explants, was appreciated also at 4 dpi in mock infected explants. Similarly, to what mentioned above for the apparent increase in apoptotic profiles in one of the mock replicate at 4 dpi, also in this case, the evidence of increased CC3 expression, in the absence of any obvious bacterial or fungal contamination, could be related to culture conditions or pre-existent, albeit very minimal (given the absence of any obvious damage to epithelium), epithelial alterations while the animal was still alive. Handling procedures during the collection of the explant should also need to be considered.
As a more general consideration, the increase in CC3 expression following EIV infection, particularly in light of the concurrent progressive decrease of NP, may offer an interesting interpretation of apoptosis as a key mechanism in accelerating virus removal. According to Nogusa, et al. (2016), apoptosis mediated by receptor-interacting serine/threonine-protein kinase 3 (RIPK3) had been proven to play a crucial role in antiviral immunity, at least in a murine model, and in this perspective apoptosis could represent a critical mechanism to contain viral infection and to accelerate its resolution.

Ki 67 increased in EIV infected explants up to 3 dpi, where the difference between mock and infected explants appeared to be statistically significant, to drop down to mock level at 5 dpi. Therefore, the regenerative processes appeared to occur concurrently to apoptotic processes, in contrast to what described by Gonzalez, et al. (2014) in canine explants where a high number of Ki67 was detected from 3 dpi onwards (however no proper quantification was performed).
Two statistically non-significant, relatively small increases were observed at 2 and 4 dpi in the mock explants, and, similarly to what considered for CC3, potentially attributed to culture conditions. Therefore, taking into account that the tracheal explant system is a very well established EVOC system, however considering - at least in the set of samples used for my research – the existence of minimal changes in a restricted number of mock samples, a careful review of

culture conditions may need to be considered to improve the system and minimise their possible impact to the overall tissue morphology.

Given the very encouraging results obtained by the application of ImageJ, I decided to additionally investigate and to quantitatively analyse the innate immunity dynamics by Mx1 expression.
Mx1 is known to play a central role in response to viral infections and particularly (but not only) following EIV infection (Fatima, et al., 2019).
The quantification of Mx1 was then conducted as described for NP and CC3 and once again with the help provided by Daniel Goldfarb a specific macro was created to quantify Mx1 expression.
Morphologically, the protein was strictly cytoplasmic and restricted to the respiratory epithelium with a grading of staining from faint to strong.
Following quantitative analysis, Mx1 showed a peak of expression at 4 dpi in EIV infected with statistically significant and highly significant differences between mock and infected explants at 3 and 4 dpi (significant) and 5 dpi (highly significant) respectively.
A similar peak at 4 dpi, and more in general a very similar (parallel) trend of expression was seen also in mock infected explants although with a much lower magnitude.
The reason for this trend is not completely clear at this stage. However, given the presence of statically significant differences between mock and infected explants, the higher expression in infected explants should in my opinion be definitely attributed to EIV infection, also taking into account the ascertained role of Mx1 in response to EIV infection (Fatima, et al., 2019).
On the other side, the presence of Mx1 in mock explants might suggest the evidence of a residual/basal expression. In facts, it has to be pointed out that the donor pony from whom the tracheal explant had been obtained had not been kept in sterile conditions.
For this reason, exposure to infectious agents or irritants while the animal was still alive should be considered as a possible explanation for this residual expression. As an alternative explanation, the Mx1 expression seen in mock explants could be tentatively explained as a basal expression/activation in the attempt to get the tissue readily protected against possible supervening infectious/irritant agents. In addition, the possible impact exerted by sample handling at the time of collection or not yet determined culture conditions might have represented possible triggering/exacerbating factors.

5.4 Quantitative analysis – Nuclear changes

Given the very high number of pictures collected for the immunohistochemical analysis, and with the ultimate purpose of quantifying pathology, all the analysed pictures were processed with ImageJ to extract the number of epithelial nuclei and the area covered by the nuclei (nuclear area).
The ultimate aim was to quantify the reduction in cellularity in terms of reduction in the numbers of nucleated cells (less nuclei equal less cells) and to translate into measurements the nuclear changes accompanying degenerative/regenerative changes, including nuclear shrinkage/condensation.

A significant decrease in the number of nuclei was appreciated at 4 dpi in EIV infected explants. Interestingly, this timepoint appeared to occur concomitantly to the drop in CC3 and the increase in Ki67 expression and interpreted as the result of combined degenerative/regenerative changes (epithelial sloughing preceding regeneration).

The reason for oscillation in the number of nuclei observed in mock infected explants - with a first decrease appreciated at 2 dpi and a second decrease at 5 dpi - in the absence of any obvious lesion or bacterial/fungal contamination, was possibly attributed to culture conditions. Normal tissue cell turnover needs also to be considered.

Similarly, a decrease in the area covered by nuclei was appreciated in EIV infected explants at 3 dpi and appeared to be statically significant.

Interestingly and unexpectedly, a trend to increase in the nuclear area was observed in EIV infected explants at 1 and 2 dpi, however not accompanied by concurrent increase in the number of nuclei and tentatively be speculated as a consequence of EIV infection. In fact, substantial nuclear remodelling has been demonstrated following influenza A virus infection (Josset, Frobert, & Rosa-Calatrava, 2008) and possibly reflecting also in change in nuclear size.

Further investigation, however, would be required to better correlate EIV infection and nuclear size variations.

6 Limitations of the study

Overall, this thesis demonstrates the feasibility of unbiased quantification of immunohistochemical and pathological changes (in terms of nuclear variations), which in turn provides quantitative data to capture subtle changes/variations that would otherwise be difficult to detect using traditional scoring approaches. In addition, the data generated are suitable for statistical analysis.

Further work would however be required to validate this approach. In particular, to increase consistency and demonstrate reliability of this system, the same set of images could be processed with a different image analysis program to confirm obtained results. In addition, to overcome the bias due to variations in orientation of the samples on slides (horizontal vs vertical vs diagonal), acquisition of the entire tissue/explant through a slide scanner and subsequent analysis of the entire length of the epithelium would increase consistency and minimise the bias of field selection made by the operator.

Another possible future challenge, particularly in terms of potential clinical/diagnostic applications of the system, would be the use of quantification on tissues characterised by intrinsic structural complexity (parenchymatous organs as opposed to luminal organs) such as biopsies or post-mortem samples (neoplastic and/or inflammatory/degenerative lesions) rather than experimental samples.

Whether the systematic use of the software would eliminate the necessity of a second operator for validation of the measurements, the figure of the pathologist would however remain essential not only in all the steps preceding the automated analysis, including the design of the experiment, and training of the software, but also, once the acquisition of data is completed, to interpret the results obtained (Treuting & Boyd, 2019), taking into account the complexity and heterogeneity of tissues under examination. Moreover, the role of the pathologist would be crucial to check samples and to verify that tissues to be analysed would meet predefined criteria for inclusion (e.g., adequate amount of tissue made available for analysis).

Eventually, histopathological scoring in my opinion should not be simply replaced by image analysis but should be preserved as an essential preliminary complementary tool that would allow the pathologist to better train the program and identify possible outliers/abnormal tissues.

7 Conclusion

In this research project, ImageJ resulted adaptable to different scenarios and applicable to either staining quantification (pixel quantification) or nuclear count (particles count) and measurement (nuclear area).

In the case of Ki67, ImageJ allowed for an accurate quantification of stained nuclear pixels, whereas with the ‘manual’ count the positive nuclei were included in the count regardless of their staining intensity, thus generating an intrinsic bias. Similarly, for the NP and CC3, the software permitted to accurately disclose their peaks of expression (and more in general their dynamics of expression), whereas with regard to NP, the histopathological scoring only demonstrated the

presence/absence of the marker, and in the case of CC3, purely allowed a subjective estimation of percentage of positivity.
In addition, the morphological evidence of epithelial thinning and reduced cellularity also found its correspondence in reliable numbers (in terms of number of nuclei and nuclear area) following the use of ImageJ.

Whether over the course of this research project, I had the opportunity to extensively use my expertise in veterinary pathology and my previously acquired experience in immunohistochemistry, the use of the image software analysis had challenged myself in the field of quantification (the development of an unbiased methodology to quantify pathological changes) and offered me a new perspective in terms of its possible applications not only to tracheal explants, and more in general to experimental settings, but also to more exquisitely diagnostic contexts, and different tissues and organs (and of course different species).
Last, but not least the experimental system used in this study had given me the great opportunity to expand my knowledge about equine influenza viruses and more in general influenza viruses, and, although restricted to experimental settings, to examine more in depth several features of the infection, including innate immunity response.

8 References

Ackerman, A. B. (1978). Histologic Diagnostic of Inflammatory Skin Diseases. A Method by Pattern Analysis. Philadelphia: Lea & Febiger.

Brayton, C. F., Justice, M., & Montgmery, C. A. (2001). Evaluating Mutant Mice: Anatomic Pathology. Vet Pathol(38), 1-19.

Brayton, C. F., Treuting, P. M., & Ward, J. M. (2012). Pathobiology of Aging Mice and GEM: Background Strains and Experimental Design. Vet Pathol(49), 85-105.

Brown, I. H. (2000). The Epidemiology and Evolution of Influenza Viruses in Pigs. Vet Microbiol(74), 29-46.

Cellular Response to Stress and Toxic Insults: Adaptation, Injury, and Death (2015). In Robbins, S. L., Cotran, R. S., Kumar, V., Abbas, A. K., & Aster, J. C. Pathologic Basis of Disease (pp. 52-59). Philadelphia, PA: Saunders Elsevier.

Caswell, J. L., & William, K. J. (2016). Respiratory System. In Jubb, Kennedy, and Palmer's, Pathology of Domestic Animals (Vol. 2; p. 567). Elsevier.

Coburn, A. M. (2017). Molecular Determinants of Influenza A Virus Cross-Species Jumps. PhD Thesis, University of Glasgow.

Collins, T. J. (2007). ImageJ for Microscopy. BioTechniques(43), 25-30.

Crissman, J. W., Goodman, D. G., Hildebrandt, P. K., & al, e. (2004). Best Practices Guideline: Toxicologic Histopathology. Toxicol Pathol(32), 126-131.

Durham, A. E., Smith, K. C., Newton, J. R., Hillyer, M. H., Hillyer, L. L., Smith, M. R., & Marr, C. M. (2003). Development and Application of a Scoring System for Prognostic Evaluation of Equine Liver Biopsies. Equine Vet. J., 35(6), 534-540.

Fatima, U., Zhang, Z., Zhang, H., Wang, X. F., Xu, L., Chu, X., Ji, S., & Wang, X. (2019). Equine Mx1 Restricts Influenza A Virus Replication by Targeting at Distinct Site of its Nucleoprotein. Viruses, 11(12), 1114.

Gibson-Corley, K. N., Olivier, A. K., & Meyerholz, D. K. (2013). Principles for valid histopathologic scoring in research. Veterinary pathology, 50(6), 1007–1015.

Gonzalez, G., Marshall, J. F., Morrell, J., Robb, D., McCauley, J. W., Perez, D. R., Murcia, P. R. (2014). Infection and Pathogenesis of Canine, Equine, and Human Influenza Viruses in Canine Tracheas. Journ of Virol, 16(88), 9208-9216.

Grant Maxie, M., & Miller, M. A. (2016). Introduction to the Diagnostic Process. In Jubb, Kennedy,and Palmer's, Pathology of Domestic Animals. (Vol. 1; pp. 1-3). Elsevier.

Josset, L., Frobert, E., & Rosa-Calatrava, M. (2008). Influenza A Replication and Host Nuclear Compartments: Many Changes and Many Questions. J. Clin. Virol, 43(4), 381-390.

Janke, L. J., Ward, J. M. and Vogel, P. (2019) 'Classification, Scoring, and Quantification of Cell Death in Tissue Sections', Vet Pathol, 56(1), pp. 33–38.

La Perle, K. M. (2019). Comparative Pathologists: Ultimate Control Freaks Seeking Validation! Vet Pathol, 1(56), 19-23.

Maglennon, G. A., Murphy, S., Adams, V., Miller, J., Smith, K., Blunden, A., & Scase, T. J. (2008). Association of Ki67 Index with Prognosis for Intermediate-Grade Canine Cutaneous Mast Cell Tumours. Vet Comp Oncol, 6(4), 268–274.

Merriam-Webster, Incorporated. (2020). https://www.merriam-webster.com/dictionary/pathology. Retrieved 2020

Miller, M. A., & Zachary, J. F. (2017). Mechanisms and Morphology of Cellular Injury, Adaptatiopn, and Death. In J. F. Zachary, Pathologic Basis of Veterinary Disease (p. 25). Elsevier.

Mitchell, R. N. (2014). The Cell as a Unit of Health and Disease. In V. Kumar, A. K. Abbas, & J. C. Aster, Robbins & Cotran Pathologic Basis of Disease. Philadelphia, United States: Elsevier.

Muranaka, M., Yamanaka, T., Katayama, Y., Niwa, H., Oku, K., Matsumura, T., & Oyamada, T. (2012). Time-related Pathological Changes in Horses Experimentally Inoculated with Equine Influenza A Virus. J. Equine Vet. Sci., 23(2), 17–26.

Nogusa, S., Thapa, R. J., Dillon, C. P., Liedmann, S., Oguin, T. H., 3rd, Ingram, J. P., Rodriguez, D. A., Kosoff, R., Sharma, S., Sturm, O., Verbist, K., Gough, P. J., Bertin, J., Hartmann, B. M., Sealfon, S. C., Kaiser, W. J., Mocarski, E. S., López, C. B., Thomas, P. G., Oberst, A., … Balachandran, S. (2016). RIPK3 Activates Parallel Pathways of MLKL-Driven Necroptosis and FADD-Mediated Apoptosis to Protect against Influenza A Virus. Cell Host Microbe, 20(1), 13–24.

Nunes, S. F., Murcia, P. R., Tiley, L. S., Brown, I. H., Tucker, A. W., Maskell, D. J., & Wood, J. L. (2010). An ex vivo swine tracheal organ culture for the study of influenza infection. Influenza Other Resp, 4(1), 7–15.

Schneider, C. A., Rasband, W. S., & Eliceiri, K. W. (2012). NIH Image to ImageJ: 25 years of image analysis. Nat. Methods, 9(7), 671–675.

Sellers, R. S. (2012). The Gene or Not the Gene—That Is the Question: Understanding the Genetically Engineered Mouse Phenotype. Vet Pathol, 49(1), 5–15.

Shott, S. (2011). Statistics Simplified: Designing Studies that Answer Questions. J Am Vet Med Assoc(238), 55-58.

Treuting, P. M., & Boyd, K. L. (2019). Histopathological Scoring. Vet Pathol, 56(1), 17–18.

Vascellari, M., Giantin, M., Capello, K., Carminato, A., Morello, E. M., Vercelli, A., Granato, A., Buracco, P., Dacasto, M., & Mutinelli, F. (2013). Expression of Ki67, BCL-2, and COX-2 in Canine Cutaneous Mast Cell Tumors: Association With Grading and Prognosis. Vet Pathol, 50(1), 110–121.

Webster, R. G., Bean, W. J., Gorman, O. T., Chambers, T. M., & Kawaoka, Y. (1992). Evolution and Ecology of Influenza A Viruses. Microbiol. Rev., 56(1), 152–179.

Wikimedia Foundation Inc. (2020). https://en.wikipedia.org/wiki/ImageJ. Retrieved 2020

Zeiss, C. J., Ward, J. M., & Allore, H. G. (2012). Designing Phenotyping Studies for Genetically Engineered Mice. Vet Pathol, 49(1), 24–31.